

PETROLOGY AND GEOCHEMISTRY OF SHEETED DYKES AND PILLOW LAVAS FROM THE SABZEVAR OPHIOLITIC MELANGE (NORTHEAST IRAN): NEW CONSTRAINTS FOR THE LATE CRETACEOUS EVOLUTION OF THE NEO-TETHYS OCEANIC BASIN BETWEEN THE CENTRAL IRANIAN MICROCONTINENT AND EURASIA

Zahra Rezaei*, Moussa Noghreyan*[✉] and Emilio Saccani**

* Department of Geology, Faculty of Sciences, University of Isfahan, Iran.

** Department of Physics and Earth Sciences, University of Ferrara, Italy.

✉ Corresponding author, email: moussanoghreyan@yahoo.com

Keywords: *Ophiolite, continental arc, Sabzevar, Late Cretaceous, Iran.*

ABSTRACT

The Sabzevar ophiolite-bearing mélangé mainly includes tectonic slices of ophiolites regarded as remnants of the Late Cretaceous oceanic basin located between the northern margin of the Central Iran Microcontinent and the southern margin of the Turan (Eurasia) plate, as well as remnants of its northern continental margin. We present here new mineral chemistry and whole rock chemical data on the sheeted dyke complex and pillow lavas series from this ophiolite. The sheeted dykes consist of basalts and basaltic andesites showing island arc tholeiitic (IAT) affinity (Group 1). They display low TiO₂ (0.37-0.81 wt%) contents and N-MORB normalized incompatible element patterns featuring Th enrichment and Ta and Nb depletion. The pillow lavas show different chemical features compared to the sheeted dykes and can be subdivided in two distinct geochemical groups. The first Group of pillow lavas (Group 2) mainly consists of andesites showing a clear calc-alkaline (CA) affinity with low TiO₂ (0.71-0.81 wt%) contents. Their N-MORB normalized incompatible element patterns display marked enrichments in Th, U, La, and Ce, and depletion in Ta, Nb, and Ti. The second Group of pillow lavas (Group 3) is mainly represented by alkaline basalts with high TiO₂ (1.54-3.45 wt%) contents. N-MORB normalized incompatible element patterns show significant Th, Ta, and Nb enrichments.

Trace element modeling shows that CA primary melts were generated by 20% partial melting of a depleted lherzolite mantle source that had been enriched by continental crust chemical components. IAT basalts were generated from various degrees of partial melting of either depleted lherzolitic or harzburgitic mantle sources bearing no or negligible influence from continental crust components. Alkaline basalts were generated by polybaric partial melting of an enriched within-plate oceanic mantle source. A new tectono-magmatic model that can explain the different rock association cropping out in the Sabzevar ophiolite is proposed. This model implies the existence, on the southern margin of the Turan plate during the Late Cretaceous, of a continental arc-forearc system where CA and IAT rocks were erupted, respectively. Alkaline basalts were erupted in a subduction-unrelated oceanic basin and then tectonically accreted to the forearc as a consequence of the collision between the seamount and the arc-forearc system.

INTRODUCTION

Iranian ophiolites include remnants of both the Paleozoic Tethys (Paleozoic ophiolites) and Neo-Tethys (Mesozoic ophiolites) oceanic lithosphere. Mesozoic ophiolites are widespread in Iran and have classically been divided in three groups (Takin, 1972; Stöcklin, 1974; McCall, 1997) (Fig. 1): 1) ophiolites of the Zagros Suture Zone, including the Neyriz, Kermanshah, and Sarve-Abad ophiolites, which appear to be coeval with the Oman (Samail) ophiolite emplaced onto the Arabian continental margin (e.g., Agard et al., 2005; Babaie et al., 2006; Sheikholeslami et al., 2008; Allahyari et al., 2010; 2014; Saccani et al., 2013; 2014); 2) ophiolites of the Makran accretionary prism, which include the Band-e-Zeyarat/Dar Anar and Fanuj-Maskutan complexes (e.g., Najafzadeh et al., 2008; Moslempour et al., 2015; Delavari et al., 2016; Saccani et al., 2017); 3) ophiolites and colored mélanges that mark the boundaries of the central Iranian microcontinent (CIM), including Nain, Baft, (e.g., Shafaii-Moghadam et al., 2009; 2013) Sabzevar (Shojaat et al., 2003; Omrani et al., 2013, Khalatbari Jafari et al., 2013a) and the ophiolites of the Sistan Suture zone (i.e., Tchehel Kureh, Nehbandan, Iranshahr, Tirrul et al., 1983; Saccani et al., 2010; Omrani et al., 2017). The Sabzevar ophiolitic mélangé includes a large variety of ophiolitic and high pressure-low temperature (HP-LT)

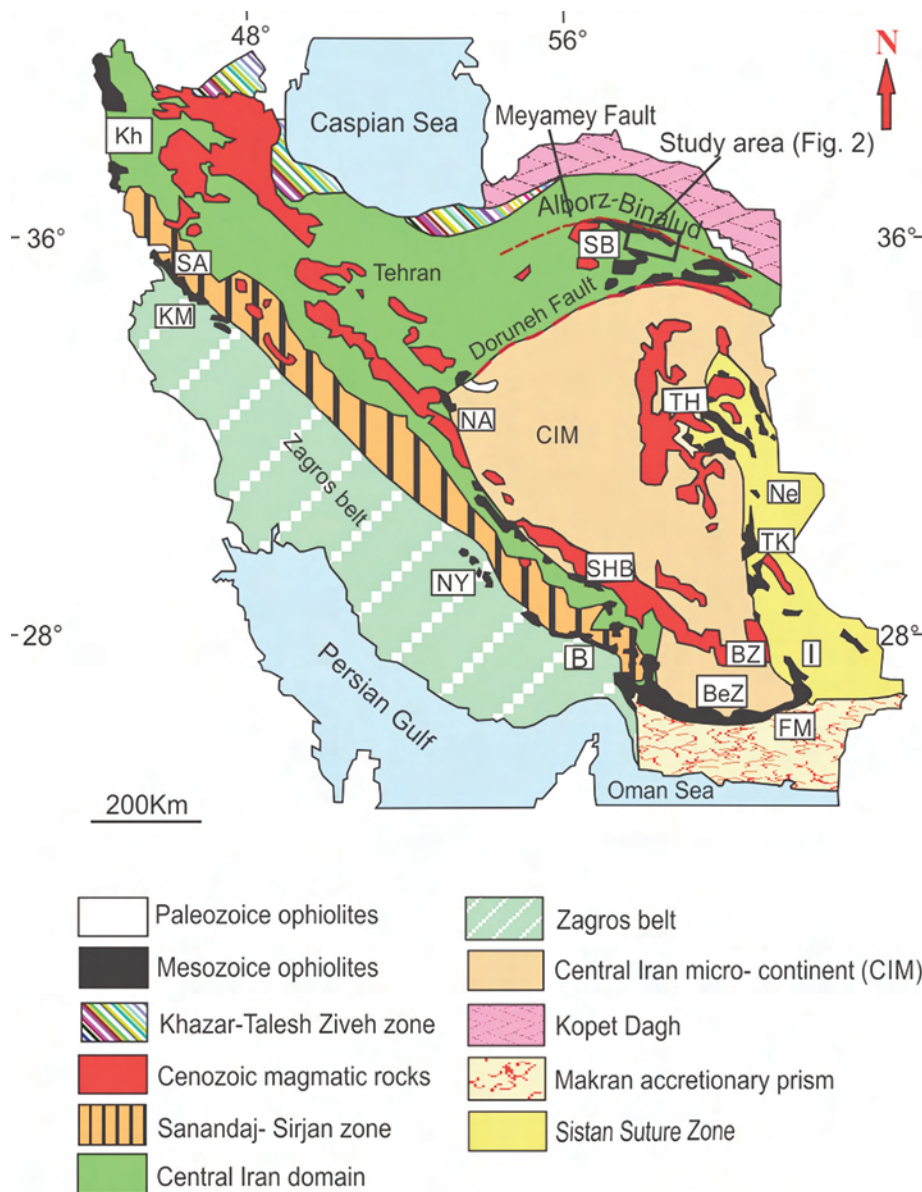
metaophiolitic rock-types (e.g., Shojaat et al., 2003; Omrani et al., 2013, and references therein). The Sabzevar ophiolitic mélangé crops out in northeastern Iran and marks the Neo-Tethys suture between the CIM, to the south, and the Turan plate (i.e., the southern margin of Eurasia), to the north (Fig. 1).

Many studies have been carried out on the lithotypes from Sabzevar ophiolitic mélangé (e.g., Alavi-Tehrani, 1976; Lensch et al., 1977; Ohnenstetter, 1983; Lindenberg et al., 1983; Spies et al., 1983; Rossetti et al., 2009; Omrani et al., 2013; Khalatbari Jafari et al., 2013a; 2013b). Lensch and Davoudzadeh (1982) identified different magmatic affinities for the magmatic rocks included within the Sabzevar ophiolitic mélangé, including mid-ocean ridge (MORB) and subduction zone affinities. Noghreyan (1982) suggested that cumulate gabbros included into the mélangé were formed from a low-Ti tholeiitic magma and concluded that the Sabzevar ophiolite formed in an immature arc setting. Based on the composition of pillow lavas, a similar conclusion was suggested by Baroz et al. (1984). Shojaat et al. (2003) investigated the petrology, geochemistry and tectonics of the Sabzevar ophiolite and identified basaltic rocks with both normal MORB (N-MORB) and enriched MORB (E-MORB) chemical signatures, as well as basaltic rocks with island arc affinity. In contrast to previous works, Khalatbari Jafari et al. (2013a) recently suggested

that the extrusive rocks of the Sabzevar ophiolitic mélangé represent oceanic crust formed at an arc-backarc transition zone. From above, it is clear that there is no general consensus on the tectono-magmatic and geodynamic significance of the Sabzevar ophiolite. In fact, different geodynamic models for the evolution of the Neo-Tethys in the northern margin of the CIM have been proposed in literature (e.g., Shojaat et al., 2003; Rossetti et al., 2009; Omrani et al., 2013). Therefore, we present new petrological and geochemical data on sheeted dykes and pillow lavas from the Sabzevar ophiolitic mélangé with the aim of constraining the petrogenetic processes and the characteristics of the mantle source involved in the sea-floor accretion in the Neo-Tethys branch north of the CIM. Finally, the data presented in this paper will also be used for testing and developing the models proposed for the evolution of this Neo-Tethys branch.

GEOLOGICAL SETTING

The Sabzevar ophiolite is the largest ophiolitic complex in northeastern Iran (Lensch et al., 1977; 1979). This ophiolite builds up an east-west trending mountain range about 200 km long and 15 to 30 km wide (Fig. 2). The Sabzevar zone is bordered to the north and south by the Meyamey and Doruneh faults (Fig. 1), respectively (Khalatbari-Jafari et al., 2013a). The Sabzevar ophiolite consists of a mélangé complex including a mixture of tectonic slices of ophiolitic and supra-ophiolitic volcano-sedimentary rocks (Khalatbari-Jafari et al., 2013a), as well as HP-LT metaophiolitic rocks (Shojaat et al., 2003). All the different chronological and lithological igneous, metamorphic (dynamothermal and ocean-floor hydrothermal) and sedimentary units and formations in this ophiolite are divided into two general genetic groups namely: the ophiolitic (Campanian-Maastrichtian)



Kh: Khoy, SA: Sarve-Abad, KM: Kermanshah, NY: Neyriz, B: Baft, SB: Sabzevar, NA: Nain, SHB: Shar Babak, TH: Torbat Hydariyeh, BZ: Bazman, BeZ: Band e Zeyarat, Ne: Nehbandan, TK: Tchehel Kureh, I: Iranshahr, FM: Fanuj-Maskutan.

Fig. 1 - Schematic tectonic map of Iran showing the distribution of the main ophiolitic complexes and the location of the study area (SB). Modified from the 1:1,000,000 magmatic map of Iran (Emami et al., 1993) and from the sedimentary-structural map of Iran (Aghanabati, 2004). The locations of the main ophiolitic complexes of Iran are shown.

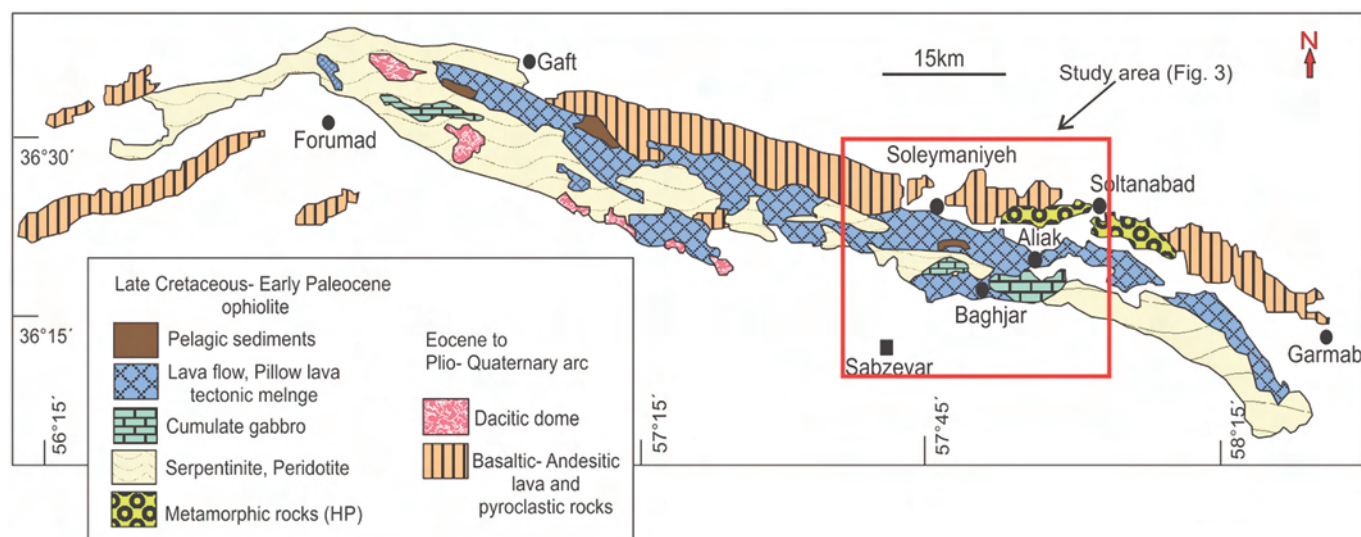


Fig. 2. Geological map of the Sabzevar area showing the location of the study area (box). Modified from the 1:1,000,000 Magmatic Map of Iran (Emami et al., 1993).

and the post- ophiolitic (Eocene- Quaternary) rock sequences (Alavi-Tehrani, 1976; Figs. 3, 4). Along the southern Doruneh fault, the Sabzevar ophiolite is strongly tectonized and consists of a mixture of serpentinites, rodingitized diabases, listvenites, altered gabbros, pillow lava fragments, exotic blocks of crystalline limestones and amphibolites. The central and northern parts of the Sabzevar ophiolite are also intensely tectonized, but thick tectonic slices preserving original internal structures can be recognized in places.

The different tectonic slices include mantle tectonites, mafic and ultramafic layered cumulates, isotropic gabbros, tonalites, plagiogranites and granophyres, sheeted dyke complex and pillow lavas interbedded with oceanic fossiliferous pelagic limestones and radiolarites (Alavi-Tehrani, 1976; Figs. 3, 4). Mantle peridotites are the volumetrically most abundant rock-type (Fig. 2) and occur as tectonic slices over the ophiolitic extrusive sequence to the south, and over the supra-ophiolitic sequence, as well as over the Paleocene-Eocene conglomerates, epiclastic breccias, and Eocene tuffs, to the north (Khalatbari-Jafari et al., 2013b). Mantle peridotites mainly consist of serpentinitized harzburgites, clinopyroxene-rich harzburgites, and lherzolites, all intruded by rodingitized individual pyroxenite and diabase dykes. Harzburgites are locally associated with chromite-bearing dunite lenses and pyroxenitic dykes (Shojaat et al., 2003; Khalatbari Jafari et al., 2013b). Tectonic slices of gabbros are delimited by fault contacts. They commonly consist of cumulate gabbros and wehrlites, which grades into isotropic gabbros and gabbronorites, and are cut by plagiogranite dykes and rare individual diabase dykes (Ohnenstetter, 1983; Khalatbari Jafari et al., 2013b). Lensch et al., (1979: 1980) suggested that the plutonic sequence was originated in an immature island arc setting.

The sheeted dyke complex crops out at the top of the plutonic crustal section of the Sabzevar ophiolite (Fig. 5a). Dykes range in thickness from 25 cm to 4 m (Fig. 5b) and extend up to 2.5 km. Dykes are characterized by increase in the grain size, from the margins toward the core of the dykes, which indicates rapid cooling along the margins (Khalatbari-Jafari et al., 2013a). They occupy radiating fractures possibly linked to conjugate faults or to extension zones varying locally. In the Soleymaniyeh area, structural

features have revealed that the shape of the magma chamber, its internal layering and the structure of the overlying sheeted dykes are mainly controlled by faults (Ohnenstetter, 1980). A highly fragmented and sheared sheeted dyke complex showing, however, clear dyke-into-dyke relationships, can be seen near Baghjar.

Pillow and massive lavas occur as tectonic slices and are predominantly gray-green in colour (Fig. 5c, d). Locally, individual diabase dikes cut the ophiolitic extrusive sequence. The main outcrops of pillow lavas are found near the Baghjar, Soleymaniyeh, and Aliak villages (Fig. 3). The few available K/Ar radiometric datings on lavas and diabases range from 81.2 ± 4.1 Ma to 76.8 ± 3.8 Ma (Lensch and Davoudzadeh, 1982). The volcanic rocks exhibit a wide compositional range including: 1) Normal and enriched MORB-like basalts (Shojaat et al., 2003); 2) within-plate alkaline basalts and trachyandesites (Shojaat et al., 2003; Khalatbari Jafari et al., 2013a); 3) IAT volcanic rocks (Shojaat et al., 2003; Khalatbari Jafari et al., 2013a). Basalts are locally intercalated with Late Cretaceous (Campanian-Maastrichtian) limestones (Shojaat et al., 2003; Khalatbari Jafari et al., 2013a).

The pillow lavas are locally overlain by Late Cretaceous-Paleocene post-ophiolitic volcano-sedimentary sequences, which were interpreted as an immature volcanic arc (Lensch et al., 1979). The Aliak unit represents the oldest unit of the volcano-sedimentary sequence. This unit is deformed into a large anticline and includes from bottom to top: lava flows, white breccias, tuffs and sedimentary rocks. The white breccias consist of lava fragments, pillow debris and, rarely, isolated pillows. The volcano-sedimentary sequence consists of tuffs interbedded with greenish litharenites and limestones. In both intrusive and volcanic rocks there is no evidence of foliation or lineation indicating regional metamorphism.

PETROGRAPHY OF THE SHEETED DYKES AND PILLOW LAVAS

Sheeted dyke complex

Dykes are hydrothermally altered under low-grade greenschist-facies condition. Alteration commonly occurs

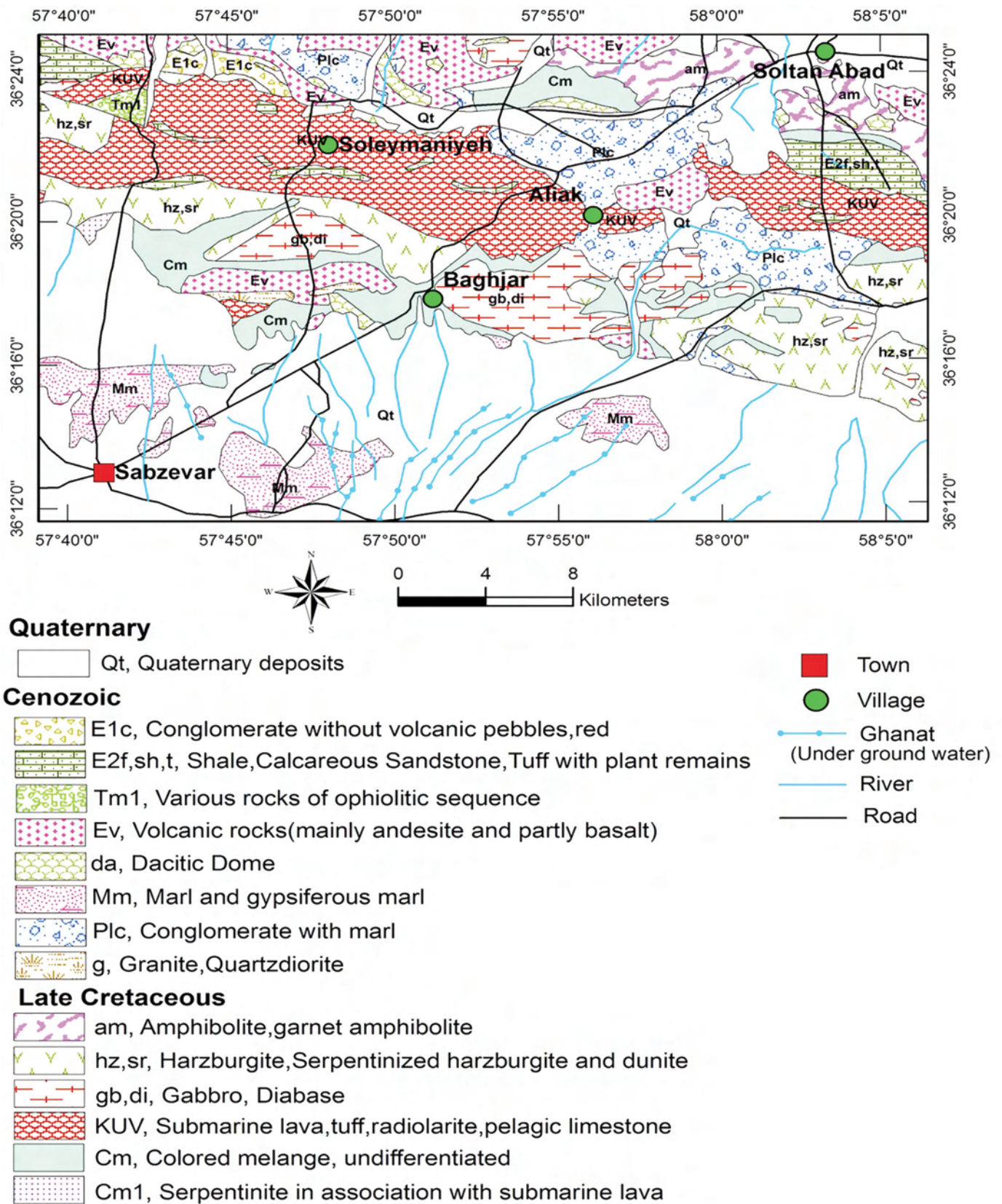


Fig. 3 - Geological map of the study area (modified from the 1:250,000 Sabzevar Geological Map, Sahandi, 1993).

through the pseudomorphic replacement of igneous phases by secondary minerals, whereas igneous textures are preserved (Fig. 5e, f). These dykes mainly consist of porphyritic basalts, basaltic andesites and andesites. Some dykes show intergranular, glomerophytic and intersertal

textures with phenocrysts of plagioclase and clinopyroxene. Clinopyroxene is partly replaced by chlorite, and occasionally by actinolite. Zeolite is also a common alteration mineral. Fine-grained Fe-oxide is a ubiquitous accessory phase.

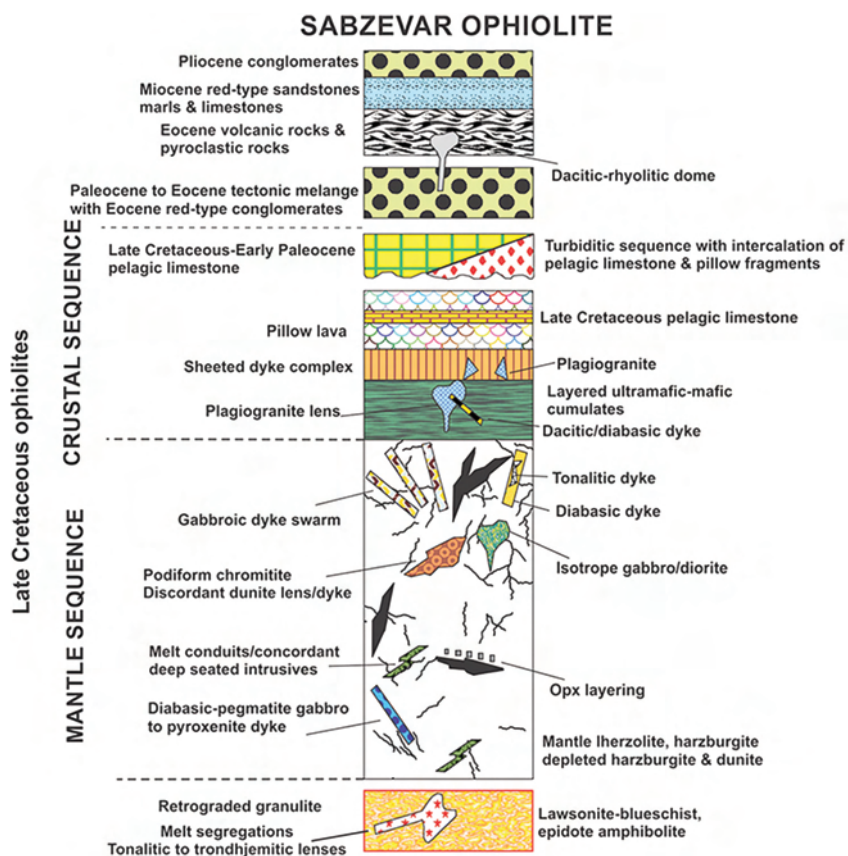


Fig. 4 - Reconstructed pseudo-stratigraphic column of the Sabzevar ophiolite showing the different lithologies of both ophiolitic mélange and supra-ophiolitic sequence (modified from Shafaii Moghadam et al., 2014).

Pillow lavas

The pillow lavas are mostly basaltic to dacitic in composition and show porphyritic and aphyric texture with microlitic, hyalo-microlitic, and interstitial groundmass. They are altered to some extent, but relict igneous textures are well preserved (Fig. 5g, h). In the porphyritic varieties, the phenocryst assemblage consists of clinopyroxene and plagioclase. In addition microphenocrysts of olivine altered in iddingsite also occur. The groundmass consists of clinopyroxene, plagioclase, Fe-Ti oxides, and minor altered, or devitrified volcanic glass. Pillow lavas usually display vesicular texture with vesicles (up to 1 cm in diameter) filled mainly with calcite, chlorite, quartz, and epidote (Fig. 5h).

ANALYTICAL METHODS

Whole-rock major and some trace element were analyzed by X-ray fluorescence (XRF) on pressed-powder pellets, using an ARL Advant-XP automated X-ray spectrometer. The matrix correction methods proposed by Lachance and Trail (1966) were applied. Volatile contents were determined as loss on ignition (L.O.I.) at 1000°C. In addition, Rb, Sr, Zr, Y, Nb, Hf, Ta, Th, U, and the rare earth elements (REE) were determined by inductively coupled plasma-mass spectrometry (ICP-MS) using a Thermo Series X-I spectrometer. The results are shown in Table 1. Moreover, for the discussion of the geochemical characteristics, major element composition has been re-calculated on L.O.I.-free bases. The accuracy of the data for XRF and ICP-MS analyses were evaluated using results for international standard rocks run as unknown. The detection limits for XRF and ICP-MS analyses were evaluated using results from several runs of twenty-

nine international standards. Results are given in Appendix A. All whole-rock analyses were performed at the Department of Physics and Earth Science, University of Ferrara.

Major element compositions of mineral phases were determined by electron microprobe spectrometry using a CAMEBAX and MS-46 in the Petrology Laboratory at the University of Nancy I in France. An accelerating voltage of 15 kV and a beam current of 10 nA were applied for 25 seconds counting interval, whereas the beam spot size was 5 μm . The major element composition was corrected using an on-line ZAF program, The results are shown in Tables 2 and 3.

WHOLE ROCK CHEMISTRY

The geochemical features of the Sabzevar pillow lavas and dykes are described here using those elements, which are virtually immobile during low-temperature alteration and metamorphism. They include some incompatible trace elements (e.g., Ti, P, Zr, Y, Sc, Nb, Ta, Hf, Th), middle (M) and heavy (H) REE, as well as some transition metals (e.g., Ni, Co, Cr, V) (Pearce and Norry, 1979). Large ion lithophile elements (LILE) and major elements are commonly mobilized during alteration (Pearce and Norry, 1979). In fact, the relative variations of Ba, Rb, SiO_2 , FeO, and CaO with respect to immobile elements (e.g., Zr, Y), indicate appreciable amounts of mobilization in many samples. Light REE (LREE) may also be affected to some degree by alteration-induced mobilization (e.g., Valsami and Cann, 1992). However, the close correlation between these elements and many immobile elements indicate that LREE have not been mobilized during the alteration processes. For example, the correlation coefficient for La-Y covariation is $r^2 = 0.92$.



Fig. 5 - Field occurrence and photomicrographs of sheeted dykes and pillow lavas: a) panoramic view of the sheeted dyke complex; b) close view of the sheeted dyke complex; c) an outcrop of pillow lavas; d) typical pillow lavas with inter-pillow carbonatic rocks; e) intergranular texture (10x); f) porphyritic texture, groundmass includes clinopyroxene, plagioclase, quartz, and opaque minerals (10x); g) microlitic and fluidal texture (10x); h) vesicular texture with vesicle filled by calcite, groundmass includes small laths of plagioclase, quartz, clinopyroxene, and opaque minerals (5x). Cpx- Clinopyroxene, Pl- Plagioclase, Opa- Opaque.

Table 1 - Major and trace element analyses of volcanic rocks and dykes from the Sabzevar ophiolite.

Rock type Unit	Group 1 Sheeted dykes									
Locality Sample Rock	Baghjar D1 bas and	Baghjar D2 bas and	Baghjar D3 bas and	Baghjar D4 bas and	Baghjar D10 bas and	Baghjar D13 bas and	Baghjar D15 bas and	Soleym. D26 bas	Soleym. D29 and	Soleym. D30 bas and
<i>XRF Analyses:</i>										
SiO ₂	53.84	55.33	53.35	53.30	53.27	55.01	52.37	51.76	56.44	55.36
TiO ₂	0.50	0.73	0.54	0.37	0.51	0.57	0.46	0.47	0.50	0.52
Al ₂ O ₃	16.91	15.37	15.90	14.97	14.28	14.24	15.46	15.15	14.24	15.93
Fe ₂ O ₃	0.68	0.88	1.15	1.00	1.38	0.93	1.60	0.83	0.66	0.80
FeO	4.52	5.87	7.66	6.65	9.19	6.20	10.69	5.51	4.40	5.31
MnO	0.08	0.11	0.15	0.18	0.15	0.13	0.07	0.10	0.07	0.16
MgO	13.06	8.36	9.82	10.50	11.28	9.93	10.39	11.30	8.68	6.62
CaO	3.64	5.96	3.69	6.61	5.51	7.50	1.96	9.28	9.67	7.47
Na ₂ O	2.49	4.41	3.18	2.43	1.17	2.75	2.20	2.43	3.58	2.98
K ₂ O	0.31	0.10	0.11	0.39	0.15	0.24	0.14	0.23	0.27	1.32
P ₂ O ₅	0.06	0.08	0.06	0.05	0.05	0.06	0.07	0.04	0.05	0.06
L.O.I.	3.98	3.01	4.37	3.78	3.21	2.51	4.66	3.06	1.48	3.49
Total	100.07	100.21	99.98	100.23	100.15	100.07	100.07	100.16	100.04	100.02
Mg#	83.7	71.7	69.5	73.8	68.6	74.0	63.4	78.5	77.8	68.9
Zn	b.d.l.	b.d.l.	b.d.l.	b.d.l.	b.d.l.	b.d.l.	b.d.l.	b.d.l.	b.d.l.	b.d.l.
Cu	b.d.l.	49	73		531	2	489	44		25
Sc	40	33	41	37	41	39	32	39	37	29
Ga	17	15	20	14	14	15	16	13	14	16
Ni	33	14	28	54	45	30	30	56	32	21
Co	34	35	38	41	47	35	48	43	35	38
Cr	129	21	89	144	92	59	45	202	84	31
V	269	271	298	268	224	263	216	217	246	252
Ba	40	48	54	31	26	29	36	31	33	61
Pb	2	2	b.d.l.	b.d.l.	b.d.l.	2	b.d.l.	3	b.d.l.	2
Rb	(ICP-MS) 0.819	(ICP-MS) 0.277	b.d.l.	(ICP-MS) 1.86	b.d.l.	(ICP-MS) 0.951	b.d.l.	(ICP-MS) 3.57	b.d.l.	(ICP-MS) 27.6
Sr	133	167	306	136	235	144	204	162	219	101
Y	11.5	16	11	15	12	18.3	13	16.7	11	11.6
Zr	32.9	49.2	44	28.6	41	33.9	48	39.2	35	36.8
La	1.56	2.17	4	4.82	4	1.69	b.d.l.	2.10	5	1.25
Ce	4.16	6.52	7	10.8	13	5.12	12	5.92	10	3.66
Pr	0.677	1.05		1.54		0.897		0.987		0.482
Nd	3.42	5.63	4	6.95	5	4.94	5	5.31	7	2.54
Sm	1.13	1.92		1.82		1.77		1.86		0.809
Eu	0.228	0.711		0.560		0.657		0.770		0.294
Gd	1.58	2.23		2.08		2.16		2.39		1.04
Tb	0.303	0.426		0.376		0.422		0.450		0.171
Dy	2.00	2.87		2.47		2.86		3.01		1.16
Ho	0.460	0.637		0.554		0.593		0.683		0.263
Er	1.35	1.61		1.58		1.86		2.06		0.734
Tm	0.209	0.271		0.233		0.275		0.307		0.116
Yb	1.35	1.84		1.60		1.91		2.10		0.788
Lu	0.204	0.276		0.243		0.287		0.299		0.124
Nb	0.736	1.37	1	0.931	2	0.960	2	0.984	2	6.29
Hf	0.270	1.58	3	0.972	b.d.l.	1.15	2	1.39	2	1.18
Ta	0.055	0.071		0.109		0.085		0.085		0.290
Th	0.232	0.545	b.d.l.	0.423	b.d.l.	0.402	b.d.l.	0.300	b.d.l.	0.279
U	0.046	0.137		0.062		0.085		0.130		0.122
Ti/V	12	17	11	9	14	13	13	13	12	13
Zr/Y	1.70	3.15	3.82	2.29	3.32	2.14	5.69	3.24	3.29	3.40
Nb/Y	0.04	0.08	0.12	0.07	0.13	0.06	0.25	0.09	0.17	0.58
Zr/Ti	0.01	0.01	0.01	0.01	0.01	0.01	0.02	0.01	0.01	0.01
(La/Sm) _N	0.89	0.73		1.71		0.62		0.73		1.00
(Sm/Yb) _N	0.93	1.16		1.27		1.03		0.98		1.14
(La/Yb) _N	0.83	0.84		2.16		0.64		0.72		1.14

bas- basalt; bas and- basaltic andesite; and- andesite; dac- dacite; trachy and- trachyandesite; b.d.l.- below detection limit. Mg# = 100 x Mg/(Mg+Fe²⁺). Fe₂O₃ is calculated assuming Fe₂O₃ = 0.15 x FeO. Normalizing values for REE ratios are from Sun and McDonough (1989). *: data from Noghrean (1982).

Table 1 (continued)

Rock type Unit	Group 1 Sheeted dykes				Group 2 Pillow lavas				
Locality Sample Rock	Soleym. 78-3-6* bas and	Soleym. 78-3-4* bas	Soleym. 6-5-7* bas and	Baghjar 78-3-45* bas and	Aliak PL21 and	Aliak PL25 and	Aliak PL26 dac	Aliak PL28 and	Aliak PL31 and
<i>XRF Analyses:</i>									
SiO ₂	51.41	51.23	53.34	54.67	65.40	62.69	67.69	64.31	64.10
TiO ₂	0.65	0.59	0.81	0.66	0.72	0.81	0.71	0.76	0.76
Al ₂ O ₃	16.44	14.04	15.49	16.23	14.24	14.81	13.13	14.17	14.19
Fe ₂ O ₃	0.84	0.96	0.86	0.95	0.55	0.63	0.46	0.60	0.47
FeO	5.61	6.37	5.73	6.33	3.65	4.22	3.07	3.97	3.14
MnO	0.12	0.16	0.11	0.12	0.10	0.10	0.09	0.11	0.08
MgO	7.39	11.07	5.08	5.45	1.98	3.11	1.43	2.57	1.79
CaO	9.02	9.31	7.54	7.89	3.05	3.15	2.69	3.34	3.97
Na ₂ O	2.93	1.65	3.44	2.90	6.35	6.71	9.36	6.58	8.88
K ₂ O	0.31	0.07	0.60	0.29	2.11	1.40	0.21	1.73	0.45
P ₂ O ₅	0.02	0.05	0.06	0.04	0.32	0.30	0.26	0.32	0.28
L.O.I.	4.35	3.72	5.91	4.27	1.59	2.18	0.97	1.64	1.91
Total	99.09	99.22	98.97	99.80	100.06	100.11	100.07	100.10	100.02
Mg#	70.1	75.6	61.2	60.6	49.2	56.8	45.3	53.5	50.4
Zn					5	17	28	8	16
Cu					17	51	48	26	33
Sc					15	17	14	16	15
Ga					17	17	15	17	20
Ni	100	291	46	33	2 b.d.l.	b.d.l.	b.d.l.	b.d.l.	b.d.l.
Co					16	20	19	17	18
Cr	265	394	80	30	17	15	17	12	15
V	203	202	233	232	112	123	134	121	161
Ba					298	199	69	254	66
Pb					3	3	4 b.d.l.		4
Rb	10	10	10	10	(ICP-MS) 31.7	19	(ICP-MS) 2.35	27	(ICP-MS) 6.37
Sr					371	303	166	350	146
Y	21	15	23	21	17.9	26	17.5	24	15.1
Zr	38	28	52	40	138	165	136	154	167
Nb	2	2	2	2	3.77	4	3.07	4	3.68
La					14.8	35	13.3	28	11.2
Ce					33.4	57	30.1	59	26.4
Pr					4.55		4.10		3.85
Nd					19.2	36	15.9	30	16.5
Sm					4.70		4.31		4.07
Eu					1.26		1.15		1.06
Gd					3.82		3.97		3.17
Tb					0.573		0.579		0.490
Dy					3.19		3.30		2.78
Ho					0.648		0.673		0.590
Er					1.76		1.90		1.54
Tm					0.272		0.290		0.235
Yb					1.75		1.94		1.53
Lu					0.250		0.297		0.217
Hf					3.96		3.78		4
Ta					0.162		0.122		0.099
Th					2.35	1	2.62	b.d.l.	1.86
U					0.711		0.880		0.945
Ti/V	20	18	22	18	39	40	32	38	29
Zr/Y	1.81	1.87	2.26	1.90	6.80	6.42	7.18	6.45	5.87
Nb/Y	0.10	0.13	0.09	0.10	0.17	0.17	0.15	0.18	0.14
Zr/Ti	0.01	0.01	0.01	0.01	0.04	0.03	0.03	0.03	0.03
(La/Sm) _N					2.03		1.99		1.78
(Sm/Yb) _N					2.99		2.47		2.95
(La/Yb) _N					6.08		4.92		5.26

Table 1 (continued)

Rock type Unit	Group 3 Pillow lavas							
Sample Rock	Baghjar PL1 bas	Baghjar PL6 bas	Baghjar PL9 trachy and	Soleym PL43 bas	Soleym PL58 bas	Soleym PL65 bas	Soleym PL82 bas	Baghjar 11-5-7* bas
<i>XRF Analyses:</i>								
SiO ₂	46.20	46.78	55.03	47.02	47.28	47.57	50.40	45.56
TiO ₂	3.36	3.45	2.35	1.61	1.54	1.87	1.83	1.77
Al ₂ O ₃	13.32	14.04	13.78	15.16	15.18	14.82	15.68	16.04
Fe ₂ O ₃	1.64	1.69	0.52	1.03	0.97	1.10	1.01	1.16
FeO	10.95	11.26	3.47	6.85	6.48	7.32	6.72	7.71
MnO	0.19	0.15	0.15	0.14	0.13	0.20	0.24	0.14
MgO	4.89	3.11	1.92	8.10	8.20	2.31	2.61	7.41
CaO	9.83	9.46	8.10	10.05	9.56	14.31	12.38	9.60
Na ₂ O	3.33	3.99	10.88	4.15	3.49	5.06	6.55	3.37
K ₂ O	2.17	1.93	0.43	0.49	1.65	1.39	0.37	2.56
P ₂ O ₅	0.65	0.75	1.18	0.36	0.40	0.51	0.51	0.49
L.O.I.	3.35	3.38	2.23	5.10	5.27	3.46	1.69	3.59
Total	99.88	99.99	100.04	100.05	100.15	99.92	99.97	99.40
Mg#	44.3	33	49.7	67.8	69.3	36	40.9	63.1
Zn	54	40	93	27	28	4	17	
Cu	23	34	b.d.l.	64	32	50	23	
Sc	33	35	13	24	26	24	24	
Ga	25	27	27	22	20	20	22	
Ni	24	29	b.d.l.	30	36	10	23	
Co	39	38	18	42	39	38	41	
Cr	59	57	6	41	36	22	27	
V	291	298	127	255	246	302	341	
Ba	378	226	335	177	333	221	122	
Pb	3	3	3	3	2	2	2	
	<i>(ICP-MS)</i>	<i>(ICP-MS)</i>	<i>(ICP-MS)</i>	<i>(ICP-MS)</i>	<i>(ICP-MS)</i>		<i>(ICP-MS)</i>	
Rb	34.3	32.94	8.86	9.88	33.1	12	6.87	45
Sr	585	443	378	509	883	937	415	
Y	37.4	31.3	51.9	27.5	18.1	22	26.2	27
Zr	240	253	457	191	166	151	167	116
Nb	55.4	49.1	81	50.5	50.0	39	44.3	28
La	32.8	31.0	59.8	34.1	30.4	31	32.4	
Ce	63.6	64.4	118	63.5	61.7	67	58.0	
Pr	7.96	8.00	14.5	7.09	6.61		6.69	
Nd	28.6	30.9	57.1	23.6	23.6	24	22.4	
Sm	7.20	7.45	13.5	5.22	4.81		4.89	
Eu	2.24	2.27	4.07	1.56	1.46		1.46	
Gd	6.05	7.01	12.4	4.51	4.26		4.14	
Tb	1.01	1.02	1.78	0.736	0.618		0.677	
Dy	5.80	5.69	9.68	4.23	3.47		3.93	
Ho	1.16	1.02	1.70	0.860	0.726		0.810	
Er	3.02	2.92	4.79	2.32	1.86		2.18	
Tm	0.420	0.391	0.622	0.332	0.265		0.313	
Yb	2.65	2.54	3.97	2.16	1.65		2.04	
Lu	0.399	0.371	0.570	0.335	0.267		0.314	
Hf	7.04	5.59	10.2	5.04	4.64		4.40	
Ta	3.32	2.48	3.79	2.84	2.88		2.57	
Th	5.04	4.41	7.66	5.38	3.89	5	5.04	
U	1.36	1.27	2.40	1.47	1.22		0.728	
Ti/V	72	72	114	40	39	39	33	48
Zr/Y	6.51	7.61	8.87	6.78	7.71	6.86	6.71	4.30
Nb/Y	1.41	1.29	1.47	1.88	2.24	1.75	1.93	1.04
Zr/Ti	0.01	0.01	0.03	0.02	0.02	0.01	0.01	0.01
(La/Sm) _N	2.94	2.69	2.85	4.22	4.07		4.27	
(Sm/Yb) _N	3.02	3.26	3.80	2.69	3.25		2.67	
(La/Yb) _N	8.90	8.77	10.82	11.34	13.21		11.40	

Table 2 - Representative analyses of clinopyroxenes in volcanic rocks and dykes from the Sabzevar ophiolite (data from Noghreyan, 1982) and estimated temperature (T°C) and pressure (GPa) of crystallization.

Rock Type	Group 1																
	Soleymaniyeheh						Baghjar										
	78-3-4 basalt		78-3-6 basaltic andesite		6-5-7 basaltic andesite		78-3-45 andesite										
21	22	25	26	27	133	134	137	138	142	146	147	74	78	80	81	82	
Mineral	50.59	52.39	52.72	53.16	51.98	53.26	52.78	52.93	52.92	50.91	51.28	52.51	51.43	52.64	52.96	52.46	52.52
SiO ₂	0.30	0.19	0.18	0.15	0.32	0.31	0.36	0.29	0.26	0.41	0.51	0.23	0.45	0.20	0.19	0.08	0.07
TiO ₂	2.13	2.31	2.31	2.13	2.39	2.48	1.99	2.32	1.97	3.56	3.13	2.60	3.50	2.36	2.28	2.16	2.55
Al ₂ O ₃	0.13	0.37	0.30	0.13	0.31	0.26	0.10	0.26	0.01	0.53	0.13	0.38	0.00	0.29	0.06	0.39	0.38
Cr ₂ O ₃	4.69	4.20	4.78	4.36	3.98	4.82	6.04	4.47	5.16	5.25	5.67	5.09	7.38	4.56	4.20	3.48	4.15
FeO	0.16	0.11	0.00	0.07	0.03	0.21	0.24	0.02	0.29	0.00	0.25	0.28	0.24	0.00	0.00	0.11	0.27
MnO	17.43	18.24	17.92	17.83	17.96	17.84	16.97	18.01	18.26	16.54	16.59	16.62	17.04	18.04	18.42	18.13	17.97
MgO	22.54	22.32	21.79	21.89	21.89	21.78	20.98	21.59	21.64	21.70	20.90	21.70	19.31	21.71	20.68	22.22	21.23
CaO	0.20	0.10	0.13	0.11	0.12	0.10	0.22	0.13	0.21	0.24	0.22	0.21	0.09	0.15	0.07	0.11	0.23
Na ₂ O	0.05	0.00	0.04	0.00	0.00	0.00	0.00	0.04	0.00	0.03	0.00	0.00	0.00	0.00	0.00	0.04	0.10
K ₂ O	98.22	100.23	100.17	98.83	98.78	101.06	99.68	100.06	100.72	99.17	98.68	99.62	99.44	100.17	98.86	98.18	99.47
Total	1.872	1.897	1.914	1.936	1.910	1.920	1.938	1.923	1.910	1.873	1.900	1.927	1.895	1.910	1.942	1.917	1.915
a.p.f.u.	0.008	0.005	0.005	0.004	0.009	0.008	0.010	0.008	0.007	0.011	0.014	0.006	0.012	0.005	0.005	0.002	0.002
Si	0.093	0.099	0.099	0.091	0.103	0.105	0.086	0.099	0.084	0.154	0.137	0.112	0.152	0.101	0.099	0.093	0.110
Al	0.004	0.011	0.009	0.004	0.009	0.007	0.003	0.007	0.000	0.015	0.004	0.011	0.000	0.008	0.002	0.011	0.011
Cr	0.158	0.093	0.066	0.033	0.059	0.037	0.031	0.043	0.081	0.081	0.047	0.024	0.039	0.071	0.001	0.067	0.066
Fe ³⁺	0.000	0.034	0.079	0.100	0.063	0.108	0.155	0.092	0.060	0.080	0.129	0.132	0.189	0.068	0.118	0.039	0.061
Fe ²⁺	0.005	0.003	0.000	0.002	0.001	0.006	0.007	0.001	0.009	0.000	0.008	0.009	0.007	0.007	0.000	0.003	0.008
Mn	0.962	0.985	0.970	0.968	0.984	0.959	0.929	0.975	0.983	0.907	0.916	0.909	0.936	0.976	1.007	0.988	0.977
Mg	0.894	0.866	0.848	0.854	0.854	0.841	0.825	0.840	0.837	0.856	0.830	0.853	0.840	0.844	0.812	0.870	0.829
Ca	0.014	0.007	0.009	0.008	0.009	0.007	0.016	0.009	0.015	0.017	0.016	0.015	0.006	0.011	0.005	0.008	0.016
Na	0.002	0.000	0.002	0.000	0.000	0.000	0.000	0.002	0.000	0.004	0.000	0.000	0.000	0.000	0.000	0.002	0.005
K	4.000	4.000	4.000	4.000	4.000	4.000	4.000	4.000	4.000	4.000	4.000	4.000	4.000	4.000	4.000	4.000	4.000
Total	0.093	0.099	0.086	0.084	0.090	0.080	0.062	0.077	0.084	0.127	0.100	0.073	0.105	0.090	0.058	0.083	0.085
Al(IV)	0.000	0.000	0.013	0.027	0.013	0.025	0.024	0.022	0.000	0.028	0.037	0.040	0.047	0.011	0.040	0.010	0.025
Al(V)	86.9	88.6	87.0	87.9	88.9	86.8	83.4	87.8	86.3	84.9	83.9	85.3	80.5	87.6	88.7	90.3	88.5
Mg#	0.00	0.05	0.05	0.04	0.09	0.08	0.12	0.08	0.08	0.07	0.10	0.05	0.08	0.05	0.05	0.02	0.02
Ti/Al	44.4	43.6	43.0	43.5	43.4	43.1	42.2	42.9	42.1	44.1	42.8	44.1	39.5	42.9	41.6	44.1	42.6
Wo (%)	47.7	49.6	49.2	49.3	50.0	49.1	47.5	49.7	49.4	46.7	47.3	47.0	48.4	49.6	51.6	50.1	50.1
En (%)	7.2	6.4	7.4	6.8	6.2	7.4	8.3	6.9	7.8	11.8	9.1	8.1	7.0	6.6	6.6	5.4	6.5
Fs (%)	0.7	0.4	0.5	0.4	0.4	0.4	0.8	0.5	0.7	0.9	0.8	0.8	0.3	0.5	0.3	0.4	0.8
Acm (%)																	
T(°C)*	1231 ± 5						1169 ± 11				1145 ± 3				1134 ± 14		
T*(°C)**	1122 ± 12						1155 ± 14				1131 ± 30				1168 ± 67		
P(GPa)*	0.32 ± 0.01						0.10 ± 0.02				0.20 ± 0.04				0.19 ± 0.02		

Wo: wollastonite; En: enstatite; Fs: ferrosillite; Acm: acmite; Mg# = 100 x Mg/(Mg + Fe³⁺ + Fe²⁺); Fe³⁺, Fe²⁺, and Fe²⁺ compositions were calculated from total measured FeO according to Droop (1987). *- estimated according to Putirka (2008); **- estimated according to Bertrand and Mercier (1985-1986).

Table 2 (continued)

Rock Type	Group 3									
Unit	Pillow lavas									
Locality	Soleymaniyeh									
Sample	11-5-7				78-3-2				0	
Rock	basalt				basalt				basalt	
Mineral	270	271	269	273	276	403	404	405	114	
SiO ₂	49.40	47.57	47.83	47.85	45.42	49.25	49.07	47.74	44.17	
TiO ₂	1.33	1.71	1.73	1.62	3.00	1.61	1.40	1.44	2.90	
Al ₂ O ₃	4.72	5.79	6.20	4.95	7.24	5.05	4.88	5.63	7.36	
Cr ₂ O ₃	0.04	0.00	0.06	0.03	0.00	0.00	0.24	0.00	0.00	
FeO	5.85	7.73	6.17	6.95	7.12	6.76	6.04	5.39	8.65	
MnO	0.15	0.00	0.11	0.01	0.10	0.32	0.00	0.30	0.18	
MgO	14.35	13.54	14.13	13.91	12.50	14.35	14.94	14.03	12.14	
CaO	23.68	23.72	22.94	22.46	23.36	21.53	22.17	22.97	22.47	
Na ₂ O	0.30	0.40	0.36	0.32	0.34	0.35	0.46	0.39	0.44	
K ₂ O	0.00	0.04	0.00	0.02	0.00	0.04	0.00	0.00	0.01	
Total	99.82	100.50	99.53	98.12	99.08	99.26	99.20	97.89	98.32	
a.p.f.u.										
Si	1.824	1.753	1.770	1.802	1.705	1.832	1.817	1.793	1.675	
Ti	0.037	0.047	0.048	0.046	0.085	0.045	0.039	0.041	0.083	
Al	0.205	0.251	0.270	0.220	0.320	0.221	0.213	0.249	0.329	
Cr	0.001	0.000	0.002	0.001	0.000	0.000	0.007	0.000	0.000	
Fe ³⁺	0.094	0.179	0.117	0.107	0.126	0.051	0.101	0.112	0.187	
Fe ²⁺	0.087	0.059	0.074	0.112	0.098	0.159	0.086	0.057	0.087	
Mn	0.005	0.000	0.003	0.000	0.003	0.010	0.000	0.010	0.006	
Mg	0.790	0.744	0.780	0.781	0.699	0.796	0.825	0.786	0.686	
Ca	0.937	0.936	0.910	0.906	0.939	0.858	0.879	0.924	0.913	
Na	0.021	0.029	0.026	0.023	0.025	0.025	0.033	0.028	0.032	
K	0.000	0.002	0.000	0.001	0.000	0.002	0.000	0.000	0.000	
Total	4.000	4.000	4.000	4.000	4.000	4.000	4.000	4.000	4.000	
Al(IV)	0.176	0.247	0.23	0.198	0.295	0.168	0.183	0.207	0.325	
Al(VI)	0.029	0.004	0.041	0.022	0.025	0.054	0.030	0.042	0.005	
Mg#	81.4	75.7	80.3	78.1	75.8	79.1	81.5	82.3	71.4	
Ti/Al	0.18	0.19	0.18	0.21	0.27	0.20	0.18	0.16	0.25	
Wo (%)	48.6	48.1	47.7	47.0	49.8	45.4	45.7	48.5	47.9	
En (%)	41.0	38.2	40.9	40.5	37.1	42.1	42.9	41.2	36.0	
Fs (%)	9.4	12.2	10.0	11.3	11.8	11.1	9.7	8.9	14.4	
Acm (%)	1.1	1.5	1.4	1.2	1.3	1.3	1.7	1.5	1.7	
T(°C)*	1171 ± 5									
T(°C)**	1195 ± 60				1082 ± 32				1230	
P(GPa)*	0.39 ± 0.03									

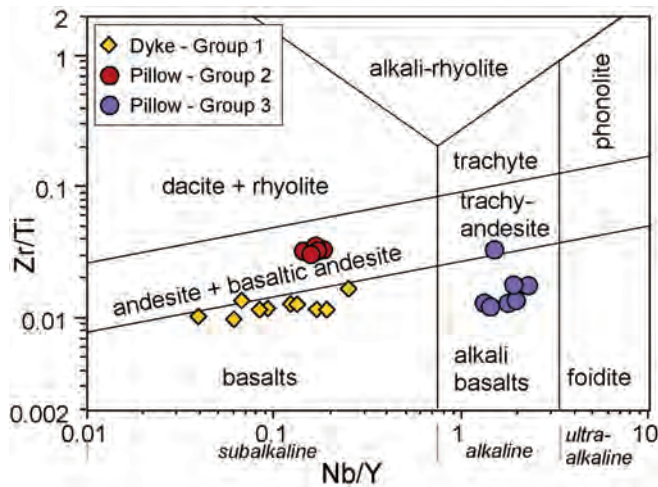


Fig. 6 - Nb/Y vs. Zr/Ti discrimination diagram of Winchester and Floyd (1977) modified by Pearce (1996) for volcanic rocks and dykes of the Sabzevar ophiolite.

Three main geochemical groups of volcanic and subvolcanic rocks can be recognized in the Sabzevar ophiolitic mélange (Table 1). Group 1 rocks are exclusively represented by dykes, whereas pillow lavas show two distinct compositions (Group 2 and Group 3). Group 1 dykes from both Baghjar and Soleymaniyeh localities show similar compositions. They are mainly represented by basaltic andesites with minor occurrences of basalts and andesites. SiO₂ contents range between 51.23 and 56.44 wt% and Mg# range between 83.7 and 60.6. These rocks display a sub-alkaline, tholeiitic nature exemplified by variable, but generally low Nb/Y ratios (Fig. 6), as well as by sharp Ti and Fe increase from basalt to andesite (Fig. 7). They are characterized by variable, but generally low TiO₂ (0.37-0.81 wt%), P₂O₅ (0.02-0.08 wt%), Zr (28-52 ppm) and Y (11-23 ppm) contents. Compatible element contents (Table 1) are very variable (e.g., Cr = 21-394 ppm). Nonetheless, these elements generally show low contents in most samples (Table 1). N-MORB normalized spider-diagrams (Fig. 8a) display

Table 3 - Representative analyses of plagioclase in volcanic rocks and dykes from the Sabzevar ophiolite (data from Noghreyan, 1982).

Rock Type Unit Locality Sample Rock Mineral	Group 1								Group 3			
	Sheeted dykes								Pillow lavas			
	Soleymaniyeh				Baghjar				Soleymaniyeh			
	78-3-4 basalt		78-3-6 basalt		78-3-45 basaltic andesite				11-5-7 basalt			
	23	24	28	30	1	72	73	76	84	272	274	275
SiO ₂	46.53	48.07	49.79	49.69	49.40	50.54	52.72	49.11	49.70	49.67	49.21	50.21
TiO ₂	0.00	0.00	0.00	0.05	0.00	0.00	0.02	0.00	0.00	0.02	0.08	0.11
Al ₂ O ₃	32.82	33.47	31.34	31.31	31.32	30.72	29.37	30.58	30.44	30.51	31.78	30.30
FeO	0.52	0.49	0.44	0.66	0.64	0.65	0.82	0.58	0.65	0.60	0.67	0.73
MnO	0.00	0.06	0.00	0.00	0.05	0.04	0.00	0.00	0.04	0.00	0.05	0.01
MgO	0.21	0.16	0.05	0.08	0.07	0.14	0.13	0.17	0.17	0.08	0.13	0.08
CaO	17.25	16.73	15.23	14.89	15.24	13.53	11.64	15.39	14.22	14.92	15.24	14.48
Na ₂ O	1.93	2.12	3.04	3.25	2.92	3.64	3.93	3.13	3.23	2.97	2.39	3.35
K ₂ O	0.00	0.00	0.01	0.00	0.00	0.02	0.50	0.00	0.02	0.28	0.29	0.21
Total	99.26	101.10	99.90	99.93	99.64	99.28	99.13	98.96	98.47	99.05	99.84	99.48
a.p.f.u.												
Si	2.162	2.185	2.280	2.277	2.271	2.321	2.412	2.277	2.306	2.297	2.258	2.311
Ti	0.000	0.000	0.000	0.002	0.000	0.000	0.001	0.000	0.000	0.001	0.003	0.004
Al	1.797	1.793	1.691	1.691	1.697	1.663	1.584	1.671	1.665	1.663	1.719	1.644
Fe ²⁺	0.020	0.019	0.017	0.025	0.025	0.025	0.031	0.022	0.025	0.023	0.026	0.028
Fe ³⁺	0.000	0.000	0.000	0.000	0.000	0.000	0.000	0.000	0.000	0.000	0.000	0.000
Mn	0.000	0.002	0.000	0.000	0.002	0.002	0.000	0.000	0.002	0.000	0.002	0.000
Mg	0.015	0.011	0.003	0.005	0.005	0.010	0.009	0.012	0.012	0.006	0.009	0.005
Ca	0.859	0.815	0.747	0.731	0.751	0.666	0.571	0.765	0.707	0.739	0.749	0.714
Na	0.174	0.187	0.270	0.289	0.260	0.324	0.349	0.281	0.291	0.266	0.213	0.299
K	0.000	0.000	0.001	0.000	0.000	0.001	0.029	0.000	0.001	0.017	0.017	0.012
Total	5.026	5.012	5.009	5.020	5.010	5.010	4.985	5.028	5.008	5.012	4.995	5.019
Ab (%)	16.8	18.7	26.5	28.3	25.7	32.7	36.8	26.9	29.1	26.1	21.7	29.2
An (%)	83.2	81.3	73.4	71.7	74.2	67.2	60.2	73.1	70.8	72.3	76.5	69.6
Or (%)	0.0	0.0	0.1	0.0	0.0	0.1	3.1	0.0	0.1	1.6	1.7	1.2

Ab- albite; An- anorthite; Or- orthoclase.

incompatible element patterns with Th relative enrichment and marked Ta and Nb negative anomalies. P and Ti also show negative anomalies, though comparatively less marked. HFSE abundance is generally low ranging from 0.3 to 0.7 times N-MORB composition (Sun and McDonough, 1989). Most samples show REE patterns (Fig. 8b) slightly increasing from LREE to HREE, as testified by the $(La/Sm)_N$ and $(La/Yb)_N$ ratios (0.6-1.0 and 0.6-1.1, respectively). By contrast, sample D4 (basaltic andesite) show both LREE/MREE and LREE/HREE enrichment ($La_N/Sm_N = 1.7$; $La_N/Yb_N = 2.2$). Eu display either slightly positive or slightly negative anomalies. The overall geochemical features of Group 1 rocks are similar to those of island arc tholeiites (IAT) from many ophiolitic complexes, as evidenced in Fig. 8a, b. Based on Th-Co covariation, Group 1 rocks can be classified as IAT (Fig. 9). Accordingly, in the discrimination diagrams in Fig. 10a they plot in the field for IAT forming in volcanic arc settings with no significant contribution from polygenetic crust (Fig. 10b).

Group 2 rocks include pillow lavas from Aliak and Baghjar localities. They are mainly represented by andesites and subordinately by basaltic andesites and dacites. SiO₂ contents range between 62.69 and 67.69 wt%, whereas Mg# range between 56.8 and 45.3. These rocks display sub-alkaline nature

as testified by low Nb/Y ratios (Fig. 6). Ti and Fe show a mild increase with increasing Zr (here used as fractionation index) (Fig. 7). Although generally low, TiO₂ (0.71-0.81 wt%) and Y (15-26 ppm) contents are comparatively higher than those observed in Group 1 rocks. In contrast, P₂O₅ (0.26-0.32 wt%) and Zr (136-167 ppm) contents are much higher than those of Group 1 rocks. Compatible element contents (Table 1) are very low (e.g., Ni < 2 ppm, Cr = 12-17 ppm). The incompatible element abundance (Fig. 8c) exhibits patterns, which are very similar to those of calc-alkaline basalts generated at active continental margins (e.g., Pearce, 1983) with marked positive anomalies in Th, U, La, and Ce, and negative anomalies in Ta, Nb, and Ti. The chondrite-normalized REE abundances (Fig. 8d) of the Group 2 pillow lavas have sub-parallel patterns, regularly decreasing from LREE to HREE. The enrichment in LREE compared to HREE is rather uniform with $(La/Yb)_N$ ratios ranging from 4.9 to 5.3. La generally varies from ~ 50 to ~ 60 times chondrite abundance. In addition, these rocks show a slight negative Eu anomaly. The REE patterns (Fig. 8d) are consistent with a calc-alkaline affinity for these rocks. In fact, Group 2 rocks plot in the field for calc-alkaline basaltic andesites and andesites (Fig. 9). Accordingly, in both the discrimination diagrams shown in Fig. 9 these samples plot in the field for calc-alkaline basalts.

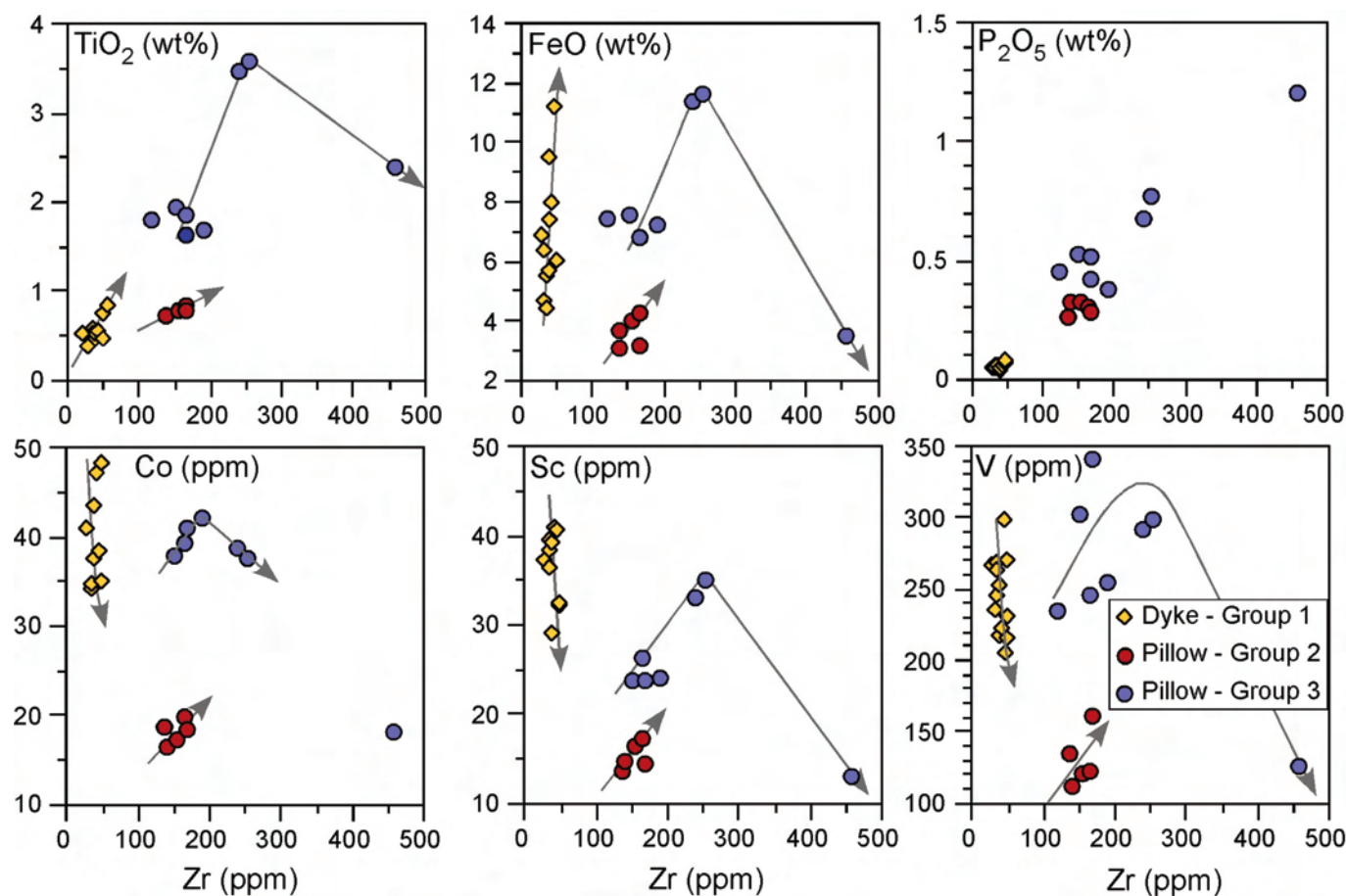


Fig. 7 - Variation in selected major and trace elements vs. Zr for volcanic rocks and dykes of the Sabzevar ophiolite. Major element oxides are recalculated on anhydrous bases. Arrows indicate inferred fractionation trends for the different volcanic and subvolcanic rock-types.

Group 3 rocks are represented by pillow lavas from Soleymaniyeh and Baghjar localities. This group mainly consists of basalts with minor trachyandesites (Table 1, Fig. 6). SiO_2 contents range between 45.56 and 55.03 wt%, whereas Mg# range from 69.3 to 33.0. The alkaline nature of these rocks is evidenced in the Zr/Ti vs. Nb/Y diagram in Fig. 6, where it can be observed that Nb/Y ratios range from 1.04 to 2.24. They are characterized by high to very high TiO_2 (1.54-3.45 wt%), P_2O_5 (0.36-1.18 wt%), Zr (116-457 ppm), Y (18-52 p.p.m.) contents, as well as Ti/V ratios (33-114). TiO_2 , FeO, Co, Cr, V, and Sc contents in basalts increase with increasing Zr values and sharply decrease in the trachyandesite sample (Fig. 7). The incompatible element abundance (Fig. 8e) is characterized by decreasing patterns, from Rb to Yb, which are similar to those of typical within-plate alkali basalts. No Th, Ta, and Nb anomalies can be seen. Only the more evolved trachyandesite sample shows slight negative anomalies in Hf and Ti, possibly reflecting the crystallization and removal of Fe-Ti phases. Group 3 rocks display significant LREE enrichment with respect to HREE (Fig. 8f), which is exemplified by their $(\text{La}/\text{Yb})_N$ ratios, ranging from 8.8 to 13.2. The overall geochemical data indicate that these rocks are very similar to that of oceanic within-plate basalts from various modern oceanic basins (e.g., Schilling et al., 1983). In fact, in the discrimination diagram shown in Fig. 10a these rocks plot in the fields for alkaline oceanic within-plate basalts forming in subduction-unrelated oceanic settings (Fig. 10b).

MINERAL CHEMISTRY AND GEOTHERMOBAROMETRY

Clinopyroxene

It is commonly accepted that clinopyroxene compositions represent a suitable indicator of the magmatic affinity of basalts from different tectonic settings (Leterrier et al., 1982), as well as from different ophiolitic types (Beccaluva et al., 1989). In fact, clinopyroxene chemistry, although controlled by crystal-chemical constrain, is strongly influenced by the composition of magmas from which they crystallize. Fresh primary clinopyroxenes were found in a few samples of Group 1 dykes and Group 3 volcanic rocks, whereas no fresh minerals were found in Group 2 rocks. Representative analyses of fresh clinopyroxene crystals are given in Table 2.

In Group 1 dykes, clinopyroxenes show augitic composition and do not show any Fe-enrichment trends from basalts to basaltic andesites (Fig. 11). Clinopyroxenes from Group 1 rocks are characterized by low TiO_2 (0.07-0.51 wt%) and Na_2O (0.07-0.24 wt%) contents, and high Mg# (80.5-90.3). Cr_2O_3 contents are rather variable and from 0 to 0.53 wt%. The Ti/Al ratio is assumed to vary as a function of the Ti-Al substitution in pyroxene which, in turn, is strongly controlled by the magma composition. Ti/Al ratios displayed by clinopyroxenes from Group 1 basalts display a wide range of variation, but are generally very low (0.02-0.12). Ti, Na and Al are negatively correlated with increasing Mg#, though

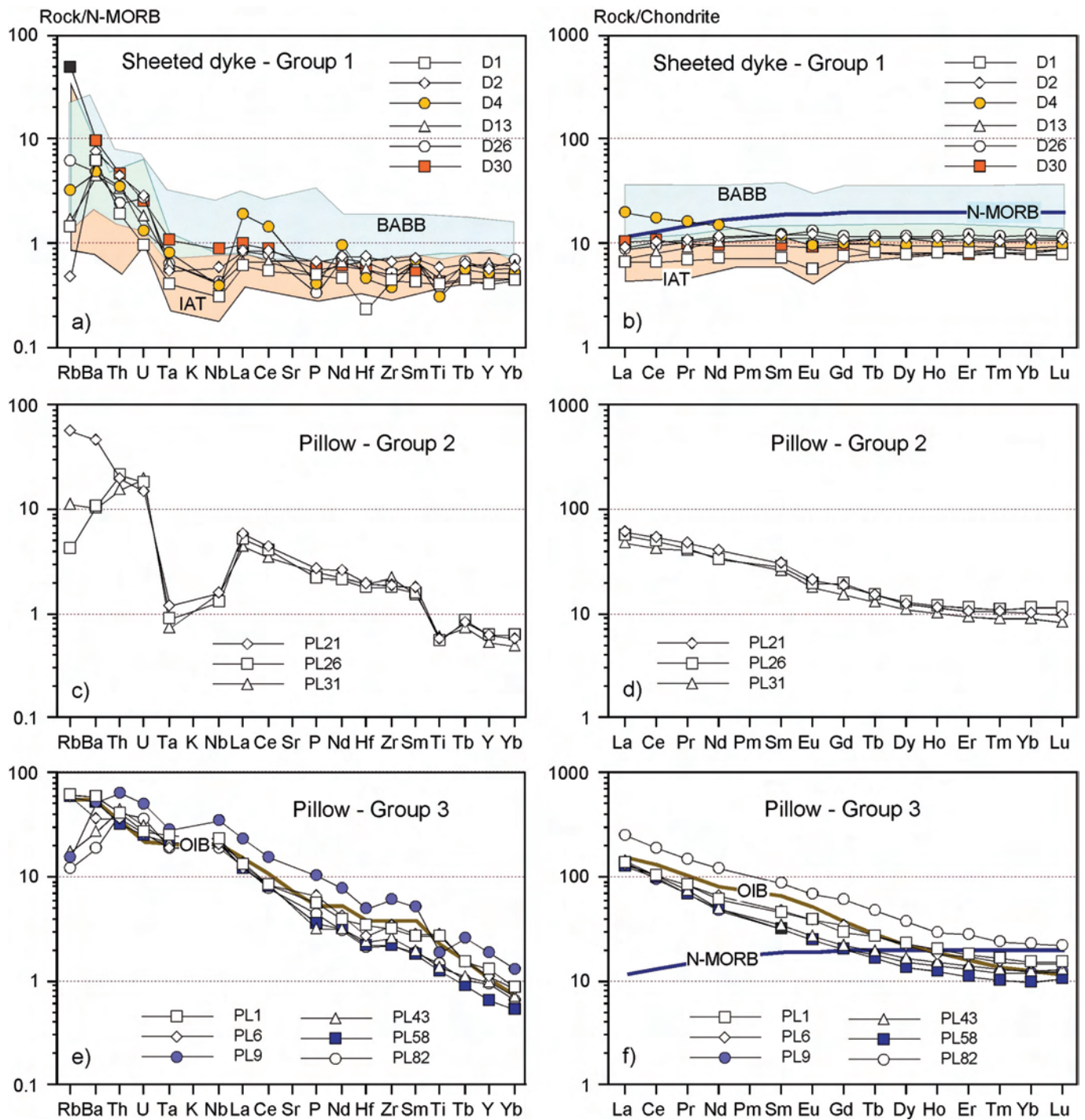


Fig. 8 - N-MORB normalized incompatible element patterns (a, c, e) and chondrite-normalized REE patterns (b, d, f) for volcanic rocks and dykes of the Sabzevar ophiolite. The composition of island arc tholeiites (IAT) from the Vourinos (Saccani et al., 2008b) and Kudi (Yuan et al., 2005) ophiolites and modern Lau Basin (Ewart et al., 1994), as well as backarc basin basalts (BABB) from the Guevgueli (Saccani et al., 2008a), Caucasus (Rolland et al., 2009), Kudi (Yuan et al., 2005), and Lau Basin (Ewart et al., 1994) are shown for comparison. Normalizing values and the compositions of modern normal-type mid-ocean ridge basalt (N-MORB) and ocean island basalt (OIB) are from Sun and McDonough (1989).

clinopyroxenes from different samples show different degree of correlations (Table 2). A marked negative correlation between Ti and Cr is also observed. Using Ti-(Ca+Na), (Ti+Cr)-Ca, and Al-Ti covariation diagrams of Leterrier et al. (1982), clinopyroxenes from Group 1 volcanic rocks plot in the fields for tholeiitic-type volcanic arc basalts (Fig. 12b). Accordingly, in the TiO_2 - SiO_2 - Na_2O discrimination diagram of Beccaluva et al. (1989) they plot in the fields for volcanic arc tholeiites and basaltic andesites/andesites (Fig. 13).

Clinopyroxenes from Group 3 basalts plot in the diopside field (Fig. 11). They show very high TiO_2 (1.33-3.00 wt%) and Na_2O (0.30-0.46 wt%) contents. Accordingly, Ti/Al ratios (0.16 to 0.27) are generally higher than those observed in Group 1 rocks. Mg# values range from 71.4 to 82.3. Cr_2O_3 show values much lower than those observed in clinopyroxene from Group 1 rocks. Except for one mineral analysis, this element is always less than 0.06 wt% (Table 2). As seen in clinopyroxenes from Group 1 rocks, Ti, Na

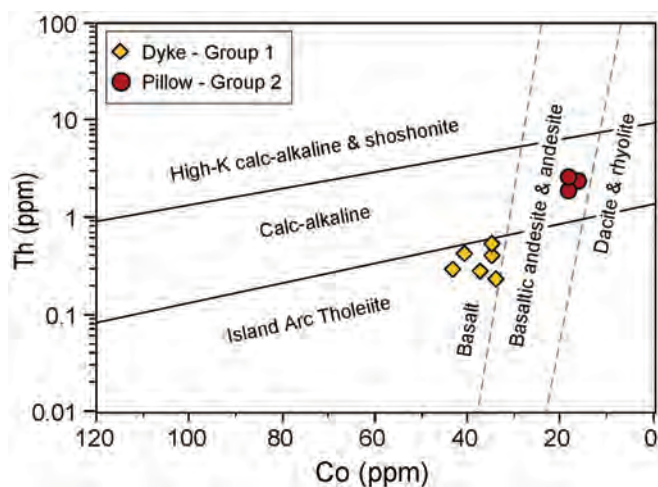


Fig. 9 - Th-Co discrimination diagram (Hastie et al., 2007) for Group 1 and Group 2 volcanic rocks and dykes of the Sabzevar ophiolite.

and Al are negatively correlated with increasing Mg#. Based on the Ti-(Ca+Na) covariation (Leterrier et al., 1982), clinopyroxene from Group 3 rocks plot in the field for alkaline basalts (Fig. 12a). In the TiO_2 - SiO_2 - Na_2O discrimination diagram of Beccaluva et al. (1989) they plot in the field for oceanic within-plate alkaline basalts (Fig. 13).

Pearce and Norry (1979) noted that Ti in clinopyroxenes

reflects the degree of depletion of the mantle source, as well as the Ti activity of the parental magma that generated the volcanic rocks. The low Ti content in clinopyroxenes from Group 1 dykes suggests that they crystallized from primary magmas generated from mantle sources, which underwent Ti removal by previous partial melting events (Hébert and Laurent, 1990). By contrast, the high Ti content of clinopyroxenes from Group 3 basalts suggests that they crystallized from primary magmas generated from mantle sources, which did not experienced previous partial melting events.

Plagioclase

Fresh plagioclase crystals were found in a few samples of Group 1 and Group 3 volcanic rocks, whereas no fresh plagioclase was found in Group 2 rocks. Representative analyses of preserved plagioclase are presented in Table 3. Plagioclases from Group 1 rocks range in composition from bytownite ($\text{An} = 72$ -83%) in basalts to labradorite-bytownite ($\text{An} = 60$ -73%) in basaltic andesites (Table 3). The plagioclases from Group 3 basalts are bytownite in composition with the anorthite content ranging from 70 to 77% (Table 2). Most of the studied plagioclases are deeply altered and, therefore, only few fresh plagioclase crystals associated with clinopyroxene can be found. Nonetheless, the anorthite contents of fresh plagioclases from Group 1 rocks plotted against the Mg# of the co-existing clinopyroxenes (Fig. 14) display compositions similar to those of SSZ-type basalts.

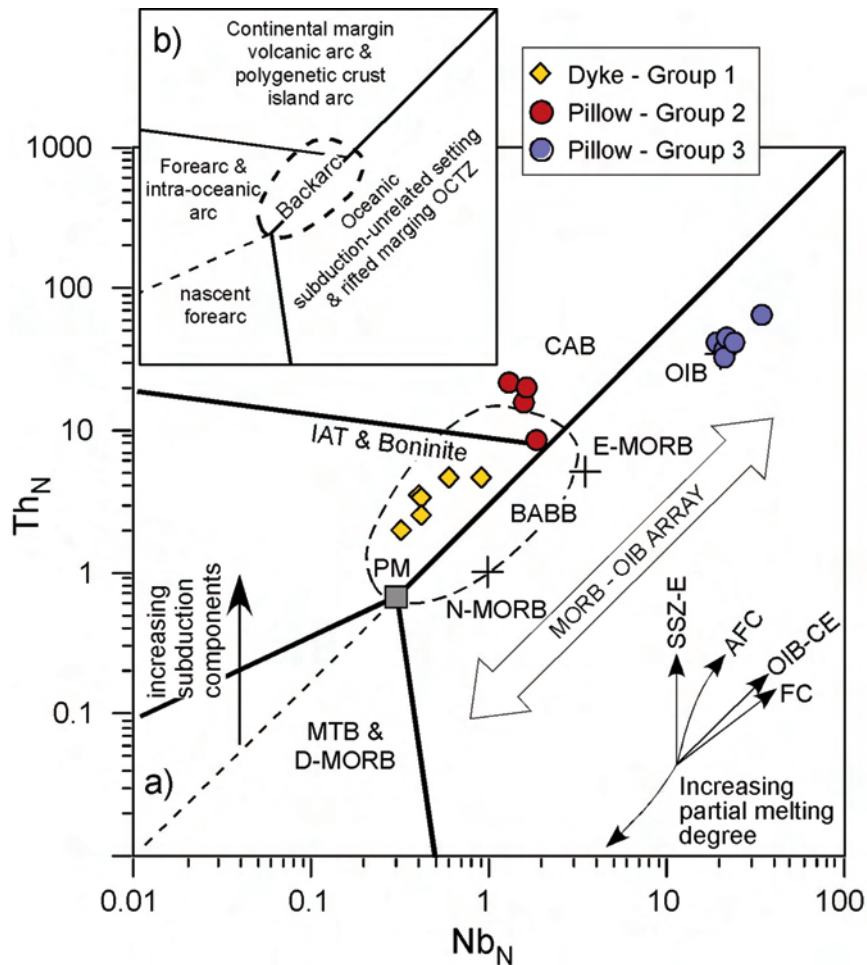


Fig. 10 - N-MORB-normalized Th vs. Nb discrimination diagram of Saccani (2015) for volcanic rocks and dykes of the Sabzevar ophiolite. a) rock types; b) tectonic setting interpretation. MORB- mid-ocean ridge basalt; N- normal type; E- enriched type; D- depleted type; IAT- island arc tholeiite; CAB- calc-alkaline basalt; OIB- alkaline oceanic within-plate basalt; BABB- backarc basin basalt; SSZ-E- supra-subduction zone enrichment; AFC- assimilation-fractional crystallization; OIB-CE- OIB component enrichment; FC- fractional crystallization. Normalization values, as well as the composition of typical N-MORB, EMORB, and OIB (crosses) are from Sun and McDonough (1989).

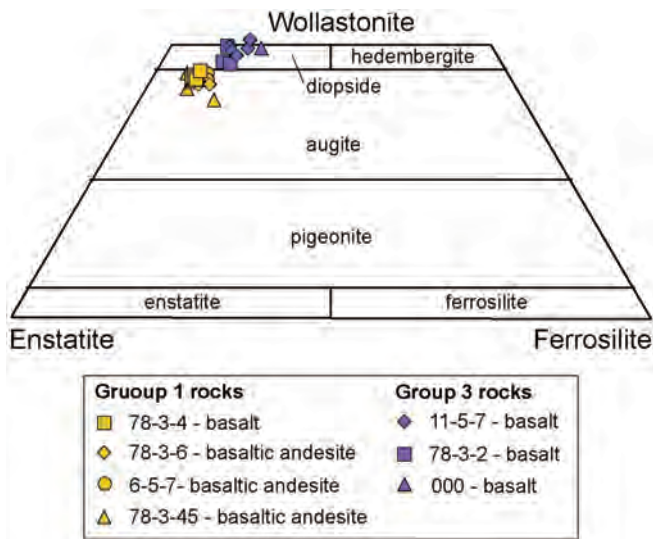


Fig. 11 - Pyroxene quadrilateral diagram (Morimoto, 1989) showing clinopyroxene compositions of volcanic rocks and dykes from the Sabzevar ophiolite.

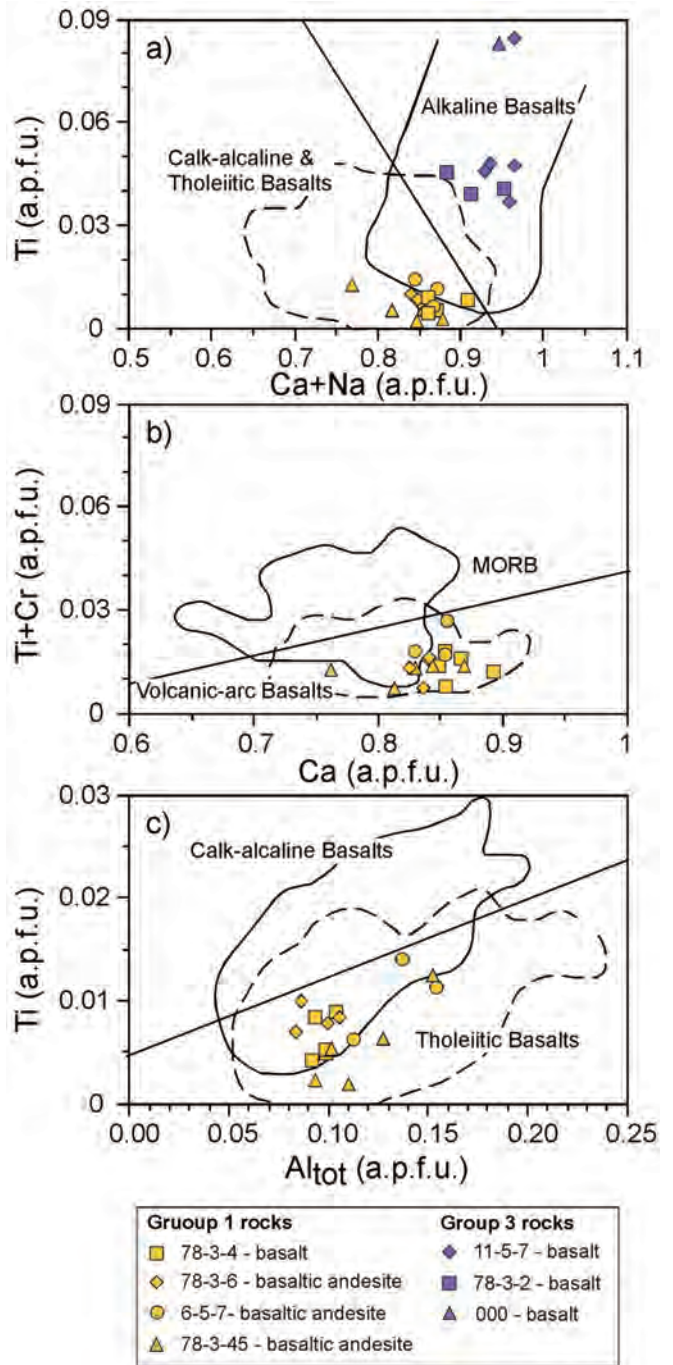


Fig. 12 - a) Ti vs. (Ca+Na); b) (Ti+Cr) vs. Ca, and c) Ti vs. Al_{tot} diagrams of Leterrier et al. (1982) showing the composition of clinopyroxenes from volcanic rocks and dykes of the Sabzevar ophiolite.

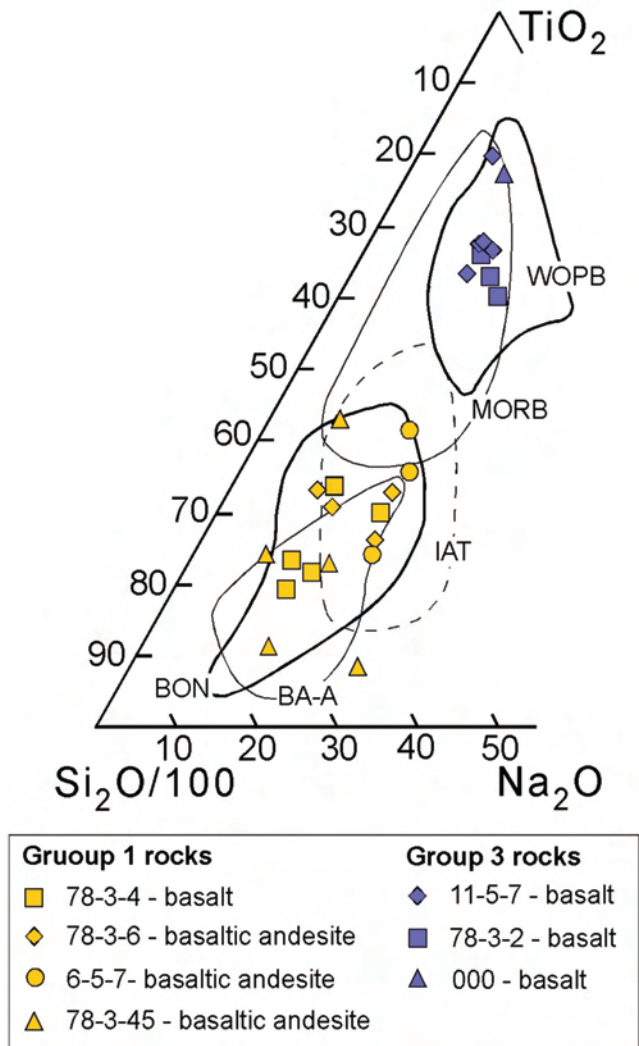


Fig. 13 - TiO₂-Na₂O-SiO₂/100 diagram for discriminating Ca-clinopyroxenes of basalts from different oceanic settings (Beccaluva et al., 1989). WOPB- within oceanic plate basalts; MORB- mid-ocean ridge basalts; IAT- island-arc tholeiites; BA-A- basaltic andesites and andesites; BON- boninites.

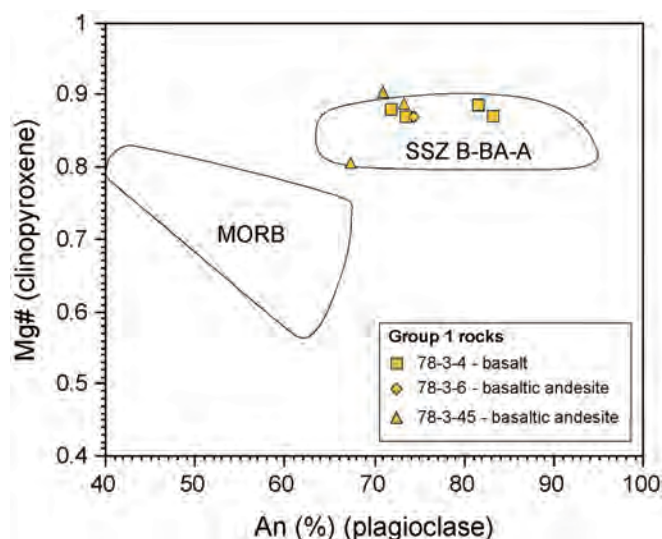


Fig. 14 - Anorthite (plagioclase) vs. Mg# (clinopyroxene) diagram for Group 1 sheeted dykes of the Sabzevar ophiolitic mélange. The compositional variation for mid-ocean ridge basalts (MORB) and supra-subduction zone (SSZ) basalts, basaltic andesites and andesites (B-BA-A), are reported for comparison (E. Saccani, personal unpublished data).

Geothermobarometry

The thermobarometric method proposed by Putirka (2008) based on clinopyroxene-whole rock equilibrium and the single clinopyroxene thermometer of Bertrand and Mercier (1985-1986) are the only methods that can be used for estimating crystallization temperatures and pressures for the studied rocks, as fresh clinopyroxene is represented in all rock-types. The different thermometers used gave very similar estimated crystallization temperatures (Table 2). Using the method proposed by Putirka (2008), the estimated magmatic temperatures for Group 1 rocks range from $1231 \pm 5^\circ\text{C}$ for the basalt to $1134 \pm 14^\circ\text{C}$ for the more evolved andesite. Interestingly, the estimated temperatures gradually decrease from basalt to basaltic andesite and andesite. Likewise, the estimated pressures broadly decrease from the basalt ($P = 0.32 \pm 0.01$ GPa) to the basaltic andesites and andesites ($P = 0.10 \pm 0.02 - 0.20 \pm 0.04$ GPa) (Table 2). The estimated temperatures obtained with the method of Bertrand and Mercier (1985-1986) gave comparable results. However, no regular decrease in temperature from basalt to andesite can be observed using this method (Table 2). According to these calculations, clinopyroxenes in Group 1 rocks were generated at depths ranging from ~ 11 km (for basalt) to ~ 3 km (for the more fractionated rocks). According to the calibration of Putirka (2008), the estimated temperatures for Group 3 basalt 11-5-7 is $1171 \pm 5^\circ\text{C}$ with a pressure of 0.39 ± 0.03 GPa (Table 2). Using the method of Bertrand and Mercier (1985-1986), clinopyroxenes from Group 3 basalts crystallized from 1230°C to 1082°C . The calculated pressure suggest a clinopyroxene crystallization at ~ 12 km depth.

DISCUSSION

Melt petrogenesis and mantle sources

As shown in the previous section, the Sabzevar ophiolite studied in this paper includes three different rock-types.

These rock-types can be used for determining the nature and tectonic significance of the magmatic events that occurred in the oceanic sector of the Neo-Tethys north to the CIM. According to Pearce and Norry (1979) and Pearce (1983), trace element (particularly, incompatible element) composition depends on the composition of mantle source and the degree of its melting rather than shallow-level crustal processes such as fractional crystallization and rock assimilation. The trace element composition of the different magma-types is therefore primarily related to different source characteristics that are associated, in turn, with distinct tectono-magmatic settings of formation. Thus, we will focus our petrogenetic discussion to the identification of the possible mantle sources and related tectonic setting of formation of the three distinct rock-groups cropping out in the dyke and pillow units of the Sabzevar ophiolite. Some trace elements contents (e.g., Nb, Th, and REE) and their degree of depletion or enrichment, as well as trace element ratios (e.g., Nb/Yb, Th/Ta, Th/Nb, Ba/Th) are moderately affected by fractional crystallization of predominantly olivine + clinopyroxene + plagioclase (Allègre and Minster, 1978). Therefore, in presence of moderate amounts of fractionation, they are believed to represent the elemental ratios in the source (e.g., Allègre and Minster, 1978; Beker et al., 1997). For this reason, the following discussion will be based on the relatively less fractionated basalts and basaltic andesites of the different magmatic groups.

A first distinction of the possible mantle sources associated with the different lava groups can be seen in Fig. 15a, which shows that Group 3 (alkaline) basalts were generated from an enriched-type mantle source, whereas, Group 1 (IAT) and Group 2 (calc-alkaline) rocks were generated from depleted-types mantle sources. Fig. 15a shows that Group 1 and Group 2 rocks plot in the fields for volcanic arc basalts and show variable extents of Th enrichment relative to Nb, which suggest variable addition of subduction-derived components. These conclusions are fully supported by the Th/Ta ratios and Zr composition (Fig. 15b). This Figure shows that the influence from subduction components is moderate for Group 1 dykes and comparatively more significant for Group 2 andesites.

We have applied trace element modelling in order to find the mantle peridotite compositions that best fit the compositions of the less fractionated basaltic rocks for each magmatic type. A rigorous quantification of the melting processes (i.e., composition of mantle sources and degrees of partial melting) generating the different rock-types is not possible as the mantle source compositions cannot be constrained in detail. However, semi-quantitative modelling of some trace elements can place some solid constraints. Due to the very different nature of Group 1 and Group 2 rocks (i.e., subduction-related), and Group 3 basalts (i.e., subduction-unrelated), we use different models.

IAT and calc-alkaline rocks are commonly interpreted as originating from partial melting of sub-arc residual peridotites that experienced Nb depletion during previous partial melting events followed by Th and LREE enrichment carried by subduction-derived fluids or melts (e.g., Pearce, 1982; 1983; Gribble et al., 1996; Parkinson and Pearce, 1998). In these settings, the fluid flux from a subducted slab may be either localized or pervasive, and fluid-mobile trace elements may be added at every melting increment (see Barth et al., 2003). In addition, compositions and the amounts of subduction-related trace elements incorporated into the overlying mantle wedge depend on a number of factors, such

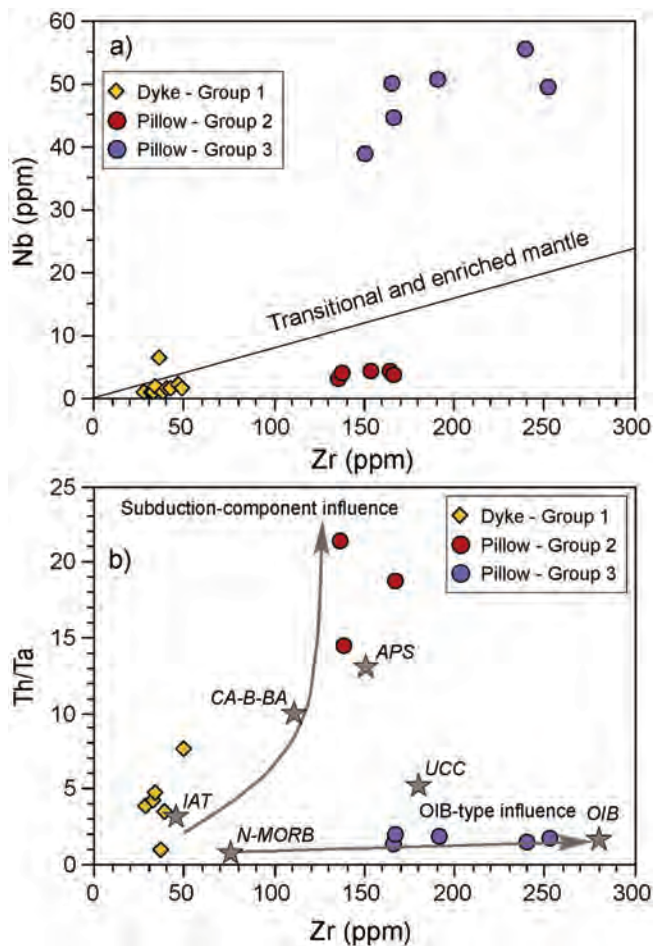


Fig. 15 - (a) Nb vs. Zr and b) Th/Ta vs. Zr diagram for volcanic rocks and dykes of the Sabzevar ophiolite. Only the relatively less fractionated basaltic and metabasaltic rocks are plotted in b). Stars indicate the compositions of: average pelitic sediments (APS); upper continental crust (UCC); average calc-alkaline basalts and basaltic andesites (CA-B-BA); average island arc tholeiitic basalts (IAT); normal-type mid-ocean ridge basalt (N-MORB); enriched-type mid-ocean ridge basalt (E-MORB); alkaline ocean island basalt (OIB). Data source: N-MORB, E-MORB, and OIB are from Sun and McDonough (1989); APS and UCC are from Taylor and McLennan (1985); IAT and CA-B-BA are calculated from 249 and 244 samples, respectively of basaltic rocks from various ophiolitic complexes (see Table 1 in Saccani, 2015 for references).

as the mineralogical compositions of the subducting rocks (in turn, mostly depending on their alteration degrees), temperatures, pressures, and distance from a subduction zone (Pearce and Parkinson, 1993; Gribble et al., 1996; Dilek and Furnes, 2011). Finally, the trade-off between the rate of extensional tectonics in the upper slab and the slab sinking is also important in facilitating fluid transfer (e.g., Flower and Dilek, 2003). Given these uncertainties, the extent and timing of fluid-induced refertilization in Th and LREE is difficult to constrain. Therefore, an alternative method for estimating the degree of depletion and degree of melting of the mantle source(s) is to plot a compatible versus an incompatible element. In fact, compatible element abundance is not significantly modified during the progressive mantle source depletion, whereas abundance of incompatible elements is closely related to source depletion and degree of melting (Pearce, 1982; 1983). To this purpose, the Cr vs. Y diagram in Fig. 16 (Pearce, 1983) is used for estimating the composi-

tion of mantle sources and the degrees of partial melting generating Group 1 and Group 2 rock-types. In this Figure, three possible mantle sources are assumed according to Murton (1989): 1) source S1 represents a MORB-type mantle source; 2) source S2 represents a depleted mantle source residual after 20% MORB-type melt extraction, which corresponds to a depleted lherzolitic composition; 3) source S3 represents a very refractory mantle source residual after 12% melt extraction from source S2 and corresponding to a fertile harzburgitic composition.

In contrast, Group 3 basalts plot along the N-MORB-OIB array (Fig. 10a) suggesting no influence from crustal material. Their composition is compatible with a genesis from primary magmas originating from enriched within-plate oceanic mantle source. In addition, the high MREE/HREE ratios displayed by these basalts (Fig. 8f) suggest an involvement of a garnet peridotite source (Beker et al., 1997). Therefore, in order to semi-quantitatively estimate the mantle peridotite composition and the degree of partial melting that best fit the composition of the less fractionated Group 3 basaltic rocks we use a melting model based on LREE/HREE (i.e., La/Yb) vs. MREE/HREE (i.e., Dy/Yb) ratios (Fig. 17), which are particularly useful for distinguishing between melting in the spinel and garnet stability fields (e.g., Thirlwall et al., 1994). This diagram has the advantage to combine two types of information in a single plot. The abundance of La is used to evaluate the enrichment of the source, whereas the Dy/Yb and La/Yb ratios are sensitive to the presence of residual garnet in the source. Partial melting of a mantle source in the spinel-facies produces little change in Dy/Yb ratios in melts with respect to melt fraction. In contrast, mantle partial melting in the garnet-facies produces large changes in Dy/Yb ratios with melt fraction. In both cases, La/Yb ratios are particularly responsive to melt fraction change (Fig. 17). Another important feature of these plots is that mixing between different melt fractions formed from garnet-facies and spinel-facies mantle will generate linear mixing arrays (see Beker et al., 1997).

Group 1

In the Cr-Y model (Fig. 16), Group 1 basalts and basaltic andesites are compatible with a wide range of mantle source compositions, as well as a wide range of partial melting degrees. Samples with the relatively higher Y contents (i.e., samples D4, D13, D26) are compatible with about 15-18% partial melting from a depleted lherzolite mantle source, residual after 20% MORB-type melt extraction (source S2). Samples with relatively lower Y contents (i.e., samples D1, D3, D10, D15, D29, D30) are compatible with > 30% partial melting of source S2, which is however an unreasonably high partial melting degree. In fact, these samples have HREE content slightly lower than samples having relatively higher Y contents (Table 1; Fig. 8b). However, modeling using HREE contents indicate that > 30% partial melting of mantle source S2 with chondrite-normalized (Sun and McDonough, 1989) $Yb_N = 1.9$ would generate concentrations of HREE in the melt that are much lower ($Yb_N = 3 - 4$) than values observed in our samples ($Yb_N = 8 - 9$). Alternatively, the Cr-Y composition of these samples can be explained assuming lower degrees of partial melting (about 10%) of a harzburgitic mantle source (source S3). Accordingly, HREE modeling assuming ~ 10% of partial melting of an harzburgitic mantle source with $Yb_N = 1.8$ would generate concentrations of HREE in the melt that are similar to those observed in basaltic andesites with comparatively lower Y contents.

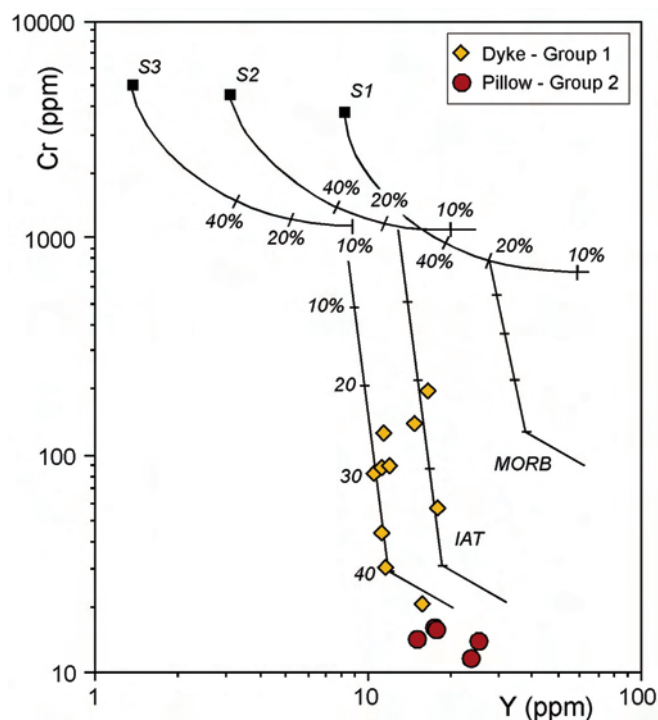


Fig. 16 - Cr vs. Y diagram of Pearce (1982) for Group 1 and Group 2 volcanic rocks and dykes of the Sabzevar ophiolite. N-MORB- normal-type mid-ocean ridge basalt; IAT- island arc tholeiite. Mantle source compositions and melting paths for incremental batch melting are calculated according to Murton (1989). S1- MORB-type mantle source; S2- residual mantle source after 20% MORB melt extraction from source S1; S3- residual mantle source after 10% melt extraction from source S2. The fractional crystallization trends are also shown (tick marks indicate 10% fractional crystallization steps).

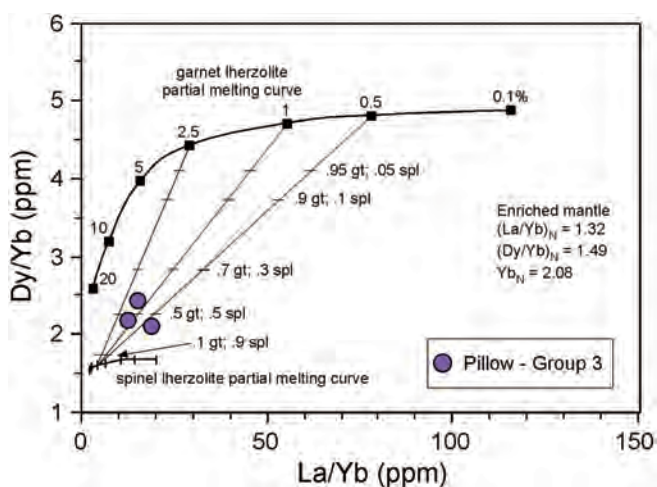


Fig. 17 - Melt curve model based on Dy/Yb vs. La/Yb applied to Group 3 pillow lavas from the Sabzevar ophiolite. Melt curves are calculated using non-modal, batch melts of a theoretical enriched (OIB-type) mantle source in the garnet- and spinel-facies lherzolitic mantle. Garnet lherzolite mode is: 0.598 ol, 0.211 opx; 0.076 cpx, 0.115 gt that melts in the proportions 0.05 ol, 0.20 opx, 0.30 cpx, 0.45 gt. Spinel lherzolite mode is: 0.578 ol, 0.270 opx, 0.119 cpx, 0.033 spl that melts in the proportions 0.10 ol, 0.27 opx, 0.50 cpx, 0.13 spl. Mantle mode and melting proportions are from Thirlwall et al. (1994). Arrays representing the mixing between various proportions of melt fractions from the garnet-facies mantle and melt fractions from spinel-facies mantle are also shown. Distribution coefficients are from Irving and Frey (1984) with the exception of those for spinel, which are from McKenzie and O'Nions (1991). Normalizing values are from Sun and McDonough (1989).

Group 1 samples show crosscutting incompatible element and REE patterns (Fig. 8a, b) suggesting that they were generated from distinct mantle sources having little differences in their trace element composition. Likewise, different $(La/Sm)_N$ ratios (0.62-1.71), as well as Th/Ta ratios (Fig. 15b) suggest that the distinct mantle sources underwent variable LREE and Th enrichments. In any case, the LREE/MREE depleted nature of most samples suggests that hydration of the sub-arc mantle wedge was accompanied by a moderate transfer of LREE-enriched subduction zone components (e.g., Barth et al., 2003). The only exception to this conclusion is represented by sample D4, which display a moderate LREE/MREE enrichment (Fig. 8b). The low fractionation of HREE with respect to MREE observed in Group 1 is consistent with melting of peridotite in the spinel-facies (see Saccani et al., 2015 and references therein). In summary, it can be postulated that the primitive magmas producing these rocks were originated from a spinel-facies depleted mantle.

Group 2

These rocks are highly enriched in Th with respect to Nb and Ta (Figs. 10, 15b) and are strongly enriched in LREE (Fig. 8d). The high abundance of LILE relative to N-MORB (Fig. 8c) clearly indicates imprints of subduction-related processes, whereas depletions in Nb, Ta, and Ti indicate a residual nature of the mantle source (Pearce, 1982). Although Group 2 rocks represent rather fractionated melts, in the model shown in Fig. 16, these rocks are compatible with about 20% partial melting from a depleted lherzolite mantle source (source S2). The marked enrichments in Th and LREE indicate that the mantle source was significantly metasomatized by subduction-related components. In fact, Fig. 15 shows that these rocks bear strong subduction-component influence, possibly related to addition of melts derived from pelitic sediments. HREE/MREE depleted patterns (Fig. 8d) are consistent with melting of peridotite in the garnet-facies (McKenzie and O'Nions, 1991). It can therefore be postulated that the primitive magmas producing these rocks were originated at depth from a depleted mantle source.

Group 3

The high MREE/HREE ratios displayed by these basalts (Fig. 8f) suggest an involvement of a garnet peridotite source (see Saccani et al., 2015 and references therein). Moreover, the high La/Yb ratios imply a source significantly enriched in LREE compared to the depleted MORB-type mantle (DMM) source. In fact, variable degrees of partial melting of a DMM source in both the spinel-facies and in the garnet-facies cannot generate the observed La/Yb and Dy/Yb ratios (not shown). In consequence, the most appropriate solution is to hypothesize a more enriched source than DMM, although it is impossible to assess the exact composition of this source. Therefore, in Fig. 17 we assume a hypothetical LREE-enriched source (Beker et al., 1997) with $(La/Yb)_N = 1.32$ and $(Dy/Yb)_N = 1.49$, and Yb concentration equal to that of DMM ($Yb_N = 2.08$). The covariation in La/Yb-Dy/Yb systematics of Group 3 basalts cannot however be explained by variable degrees of partial melting of this enriched source in either the spinel- or garnet-facies. Melting in the garnet-facies produces melts with much higher Dy/Yb ratios than those of Group 3 samples at reasonable degrees of melting (i.e., < 15%). Alternatively, the mantle source would require an unusually low Dy/Yb ratio if the samples were to be simply the product of garnet-facies mantle

melting. By contrast, melting in the spinel-facies produces melts with both La/Yb and Dy/Yb ratios lower than those of Group 3 basalts. Therefore, the simplest model to account for the REE systematics of these rocks involves mixing of small melt fractions from garnet-facies enriched mantle with relatively larger melt fractions from spinel-facies (Fig. 17). This Figure shows that the La/Yb-Dy/Yb systematics of Group 3 basalts can be explained by mixing of small degree melts (~ 0.5-2%) and larger degree melts (~ 5%) from garnet- and spinel-facies mantle, respectively. Finally, it should be noted that variations in the degree of partial melting in the spinel field are difficult to constrain due to the small range in both Dy/Yb and La/Yb ratios generated by spinel-facies melting. Some scatter in the La/Yb - Dy/Yb systematics (Fig. 17) might be accounted for by small fluctuations in the degree of melting of garnet-facies mantle. In any case, from a semi-quantitative point of view, melt fractions in the garnet field are restricted to < 2% whereas those in the spinel field are around 5%. The possible influence of crustal contamination can be excluded as the Th-Nb compositions of all rock-types plot within the MORB-OIB array (Fig. 10a). Other geochemical indicators further support this conclusion. For example, high Th/Ta and low Nb/U ratios are effective indicators of crustal contamination. Group 3 basalts show very low Th/Ta (1.35-2.02) and Nb/U (33-41) ratios. These Nb/U ratios are comparable to those of the typical OIB (Nb/U = 47) of Sun and McDonough (1989).

Tectono-magmatic significance

The petrological evidence presented in the previous section allows to conclude that the geochemically distinct groups of volcanic and subvolcanic rocks from the Sabzevar ophiolite are related to different mantle source compositions and partial melting degrees. Group 1, and Group 2 rocks were formed from primary melts generated, in turn, from depleted mantle sources that experienced variable subduction-related metasomatism prior to melting. Therefore, all these rocks were likely generated in volcanic arc tectonic settings. Nonetheless, the different nature of the inferred mantle sources associated with each single rock-group suggests that they likely represent different types of volcanic arc settings or in different portions of the same volcanic arc setting. The calc-alkaline nature and the marked influence from continental crust materials shown by Group 2 rocks (Figs. 10a and 15b) suggest formation in a continental arc tectonic setting. Calc-alkaline rocks generated in continental arc tectonic settings are not very common in ophiolitic complexes. However, some scattered occurrences of calc-alkaline rocks associated with ophiolitic sequences or included in ophiolitic mélanges are recorded from the Carpathian belt in Romania (e.g., Bortolotti et al., 2002; 2013; Nicolae et al., 2003; Ionescu et al., 2009), to the Hellenic belt in Greece (e.g., Koglin et al., 2009), the Ankara Mélange and Kızıldağ ophiolites, in Turkey (e.g., Parlak et al., 2009) and the south Caspian area in Iran (e.g., Salavati, 2008). The island arc tholeiitic affinity of Group 1 rocks and their moderate subduction-type geochemical signature suggest that these rocks were little influenced by continental crust material and likely formed in the forearc sector of a volcanic arc setting. In any case, Group 1, and Group 2 rocks represent materials incorporated into the Sabzevar ophiolite from the upper plate.

The formation of Group 3 alkaline rocks implies the occurrence of mantle sources strongly metasomatized by

OIB-type (plume type) components. Two alternative hypotheses can account for such OIB-type metasomatized mantle: 1) the existence of plume activity in the region during Cretaceous times and 2) the existence of deep mantle heterogeneously modified by previous mantle plume activity. In the first case, Group 3 basalts likely represent seamount material originated in an oceanic within-plate setting. In the second hypothesis, they may have been formed in an oceanic mid-ocean ridge setting by tapping strongly enriched local portions of a heterogeneous mantle, as documented in some Mediterranean Tethys ophiolitic complexes (e.g., Bortolotti et al., 2017). Alternatively, they may represent volcanic rocks erupted at ocean-continent transition zones during the continental rift phase preceding the oceanic spreading, as observed in many Mediterranean Tethys ophiolitic complexes (e.g., Saccani et al., 2003; 2015). Nonetheless, the petrogenetic mechanism for the formation of Group 3 rocks implies polybaric partial melting starting in the deep mantle and continuing in the shallow level mantle. Such a mechanism is commonly observed in within-plate tectonic settings and in continental rift settings, whereas is rarely observed in mid-ocean ridge settings (see Saccani et al., 2015 and references therein). It follows that Group 3 alkaline basalts were likely formed in seamount setting. The data presented in this paper do not allow a conclusive identification of the original tectonic setting of formation of these basalts to be made. However, in any case they represent fragments of oceanic crust that were incorporated into the Sabzevar ophiolite from the subducting plate.

Geodynamic implications

The data presented in this paper together with literature data (e.g., Baroz and Macaudiere, 1984; Lensch et al., 1977; 1979; Shojaat et al., 2003; Khalatbari Jafari et al., 2013b; Omrani et al., 2013) indicate that the Sabzevar ophiolite includes a wide range of both mantle and magmatic rocks. The geochemical and petrological diversity of these rocks suggests that several distinct tectono-magmatic events took place in the Sabzevar oceanic basin, as well as in its continental margins that is, the CIM, to the south, and the Turan plate (Eurasian plate), to the north.

Different tectonic models have been proposed in previous literature for explaining the formation of the distinct magmatic rocks in the Sabzevar ophiolite. Stöcklin (1974) argued that the Sabzevar ophiolite represents remnants of the Sabzevar basin, which was a branch of the Neo-Tethys Ocean that formed between the CIM (to the south) and the Eurasian plate (to the north) during the Early Jurassic and reached its maximum extent during the Late Cretaceous. Sengor (1990) suggested that the Sabzevar Ocean was the northern part of a seaway that entirely surrounded the CIM. The other parts are (Fig. 18a): 1) the Fanuj (Makran) Ocean, which was located on the west-southwest and separated the CIM from the Sanandaj-Sirjan/Bajgan-Durkan blocks; 2) the Sistan Ocean that was located to the east and separated the CIM from the Afghan block.

Khalatbari Jafari et al. (2013a) suggested that the IAT and alkaline volcanic rocks of the Sabzevar ophiolitic mélange were originated in a backarc tectonic setting developed in the Late Cretaceous, whereas the sheeted dyke complex was formed in a forearc setting. Rossetti et al. (2009), studying upper Early Cretaceous (107 Ma) migmatitic mafic granulites cropping out along the northern margin of the Sabzevar ophiolite, suggested that these rocks formed during

that the subduction of the Sistan Ocean to the east of the CIM (Fig. 18a). They also concluded that the Late Cretaceous Sabzevar and Nain ophiolites (Fig. 18a) were originated in a backarc basin associated with the subduction of the Sistan Ocean. This conclusion is based on the assumption that the Sabzevar and Nain ophiolites are parts of the same unit, and formed in a Late Cretaceous backarc basin, which closed during the Paleocene-Eocene subduction of the Arabian plate under the Iranian plate.

In contrast, Baroz et al. (1984) and Lensch et al. (1979; 1980) studying the middle part of the Sabzevar ophiolite at-

tributed the composition of pillow lavas to an immature island arc and suggested these ophiolites represent remnants of an active margin. Accordingly, Shojaat et al. (2003), studying the petrology and geochemistry of the volcanic rocks in the Sabzevar ophiolite, proposed that this ophiolite was formed in a subduction-related setting as a consequence of the closure of the Sabzevar Ocean through a northeast-dipping subduction zone. Similar conclusions were obtained by Omrani et al. (2013), who studied the high pressure-low temperature metamorphic rocks (i.e., blueschists) cropping out in the northern part of the Sabzevar ophiolite.

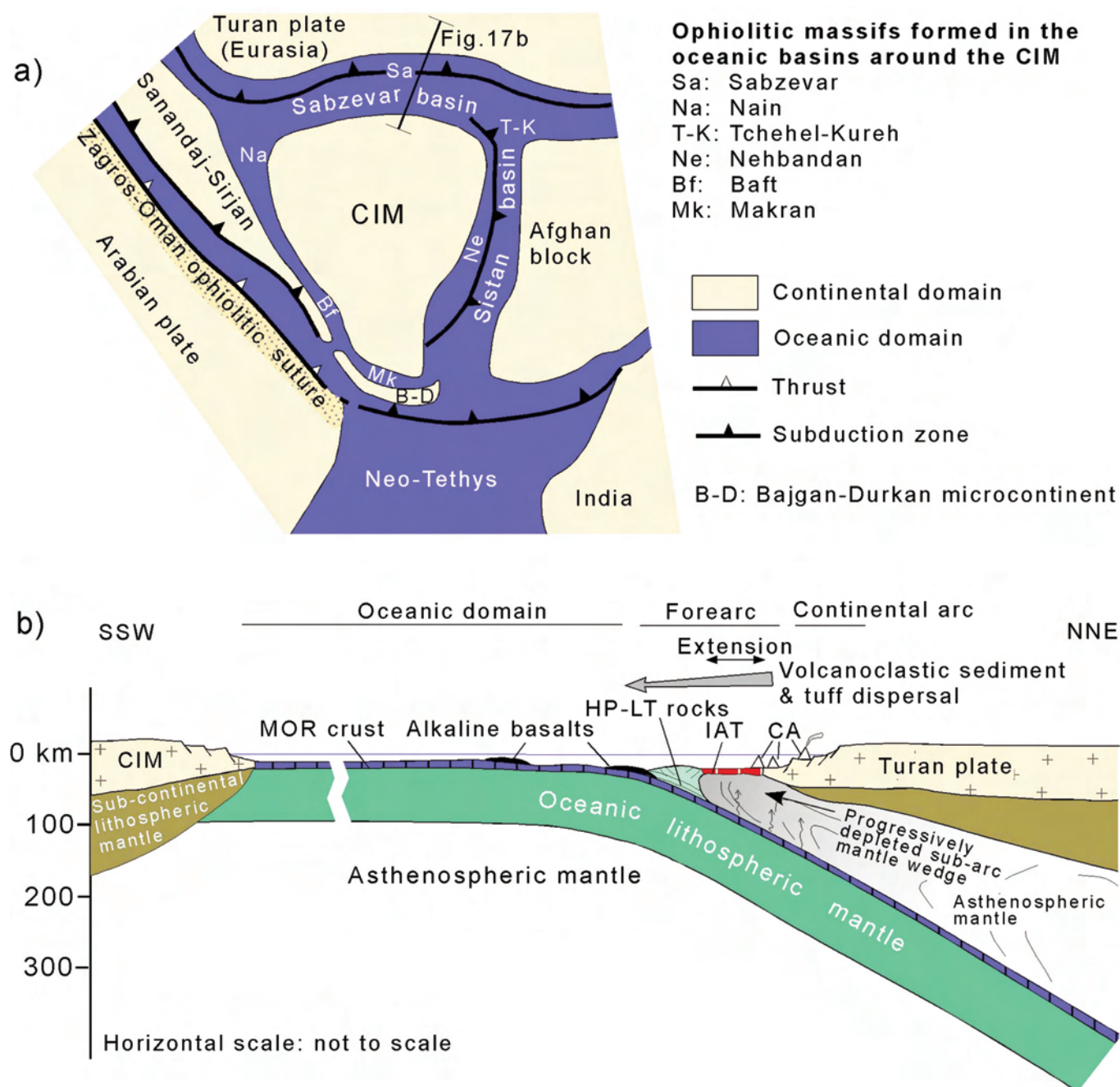


Fig. 18 - a) Schematic tectonic framework of the Central Iran microcontinent (CIM) and surrounding oceanic and continental areas during the Late Cretaceous; b) two-dimensional geodynamic reconstruction of the transect across northern CIM - Sabzevar oceanic basin - southern N Iran (Eurasia) continental margin at Late Cretaceous times. Both figures were drawn based on models proposed by Shojaat et al. (2003); Saccani et al., (2010; 2014); Omrani et al. (2013); Allahyari et al. (2014). MORB- mid-ocean ridge; HP-LT- high pressure-low temperature; IAT- island arc tholeiite; CA- calc-alkaline.

From the above outline of the tectonic models previously proposed in literature, it is quite clear that there is no general consensus about the tectonic setting of formation of the Sabzevar ophiolite. The new data presented in this paper allow us to discuss and improve the tectonic models so far presented. A possible tectono-magmatic model that can explain the formation of the different magmatic rock-types in the Sabzevar ophiolite is shown in Figure 18b. In this model, a northward subduction the Sabzevar Ocean below the southern margin of the Turan plate (Eurasia) is assumed according to Shojaat et al. (2003) and Omrani et al. (2013). No data allow the age of the inception of the subduction and associated arc magmatism to be defined in detail. Therefore, we reasonably assume that the subduction started between the Middle and Late Cretaceous (not shown). The chemistry of IATs indicates that tectonic setting of formation was characterized by no or negligible chemical influence from continental crust components (Fig. 15b). This implies that IATs formed onto oceanic crust in the forearc sector of a continental arc during Late Cretaceous (Figs. 18b). IATs are represented by plutonic rocks (see Lensch et al., 1979; 1980), as well as by sheeted dykes. This suggests that the forearc setting was characterized by extensional tectonics, as observed in many Tethyan ophiolitic complexes (e.g., Dilek and Furnes, 2011). In contrast, the chemistry of calc-alkaline volcanic rocks indicates that they have been strongly influenced by continental crust chemical components (Figs. 15b), suggesting that these rocks were erupted onto the southern realm of the Turan continental domain.

Khalatbari Jafari et al. (2013a) suggested that the alkaline basalts of the Sabzevar ophiolite were originated in a backarc tectonic setting. This conclusion is mainly based on the occurrence, in the Afchang area (~ 15 km to the west of Soleymaniyeh), of alkaline basalts covered by volcanoclastic sedimentary rocks intercalated with tuffs showing characteristics of subduction zone volcanism. However, these alkaline basalts are found as tectonic slices, which are sandwiched between harzburgitic tectonic masses. The tectonic contacts between basalts and peridotites are characterized by the occurrence of small tectonic slices of pelagic sediments in between. In addition, in the areas studied in this paper, the alkaline pillow lavas are not associated with the volcanosedimentary sequence described by Khalatbari Jafari et al. (2013a). Alkaline volcanic rocks are very common in many supra-subduction zone (SSZ) ophiolites or ophiolitic mélanges as, for example, in the Dinarides (e.g., Bortolotti et al., 2004; Saccani et al., 2011; Chiari et al., 2012) and Oman (Chauvet et al., 2011) ophiolites. However, these alkaline rocks are not genetically related to the SSZ ophiolites, as they represent fragments of the subduction-unrelated oceanic crust tectonically accreted to the forearc setting. Therefore, we favour the hypothesis that alkaline volcanic rocks from the Sabzevar ophiolite represent remnants of seamounts. In fact, these rocks are more buoyant than oceanic crust formed at a mid-ocean ridge and therefore they have a greater potential to be 'peeled off' and accreted on to island arcs and active continental margins. The local occurrence of subduction-related volcano-sedimentary sequences associated with seamount-type alkaline basalts can easily be explained. Once these basalts reached the trench zone and were accreted to the forearc region, they were locally covered by volcanoclastic sediments and pyroclastic deposits originated from the arc front (Fig. 18b). Likewise, although rare, the occurrence of N-MORB-type rocks

(Shojaat et al., 2003) point out for their incorporation into the accretionary wedge in the forearc region of a subduction system. In addition, the formation of high pressure-low temperature rocks (Omrani et al., 2013) is also compatible with an accretionary wedge-forearc-arc system such as that shown in Fig. 18b. Unfortunately, no chemical analyses are available on these rocks and therefore it cannot be established if they represent materials from the subducting oceanic crust or materials from the forearc dragged in depth by processes of subduction erosion of the accretionary wedge and then exhumed as HP metamorphic slices (e.g., Huene and Scholl, 1991). In any cases, the Sabzevar ophiolitic mélange bears rocks from lower and upper plate of a trench-forearc system, including the remnants of an accretionary wedge, i.e. the HP metamorphic rocks. This type of mélange typically developed during the final closure of the oceanic basin when the rocks from lower and upper plate are tectonically mixed together into the mélange.

CONCLUSIONS

The Sabzevar ophiolite represents remnants of the Late Cretaceous oceanic basin located between the northern margin of the Central Iran Microcontinent and the southern margin of the Turan (Eurasia) plate. This ophiolite consists of an ophiolitic mélange including ultramafic mantle tectonites, mafic and ultramafic layered cumulates, isotropic gabbros, plagiogranites, a sheeted dyke complex and pillow lavas interbedded with pelagic limestones and radiolarites, as well as high pressure-low temperature metamorphic rocks. In this paper, the sheeted dyke complex and the pillow lava series are investigated through mineral chemistry, geochemical, and petrological study. The main conclusions can be summarized as follows:

1) The sheeted dykes and pillow lavas include three chemically distinct groups of rocks. The sheeted dyke complex consists of basalts and basaltic andesites showing IAT affinity (Group 1). The pillow lavas include andesites and minor basaltic andesites and dacites showing a clear calc-alkaline affinity (Group 2) and basalts and very minor trachyandesites, all showing alkaline within-plate affinity (Group 3). Clinopyroxene chemistry fully supports the above conclusions for Group 1 sheeted dykes and Group 3 pillow lavas but, unfortunately, no fresh clinopyroxene minerals were found in Group 2 pillow lavas.

2) Trace element modeling shows that some of the IAT basalts were generated from relatively high degrees (15-18%) of partial melting of a depleted lherzolite mantle source, residual after 20% MORB-type melt extraction. In addition, some other IAT basalts may have been generated by relatively lower (10%) partial melting of a harzburgitic mantle source. The trace element composition of calc-alkaline primary melts is compatible with about 20% partial melting from a depleted lherzolite mantle source. REE modeling shows that alkaline basalts were generated from polybaric partial melting of an enriched within-plate oceanic mantle source that started to melt in the garnet-facies mantle and continued to melt in the spinel-facies mantle.

3) The petrological evidence suggests that both IAT and calc-alkaline rocks were generated in a subduction-related tectonic setting. The chemistry of calc-alkaline pillow lavas indicates a significant influence by continental crust chemical components, which suggest that these rocks were erupted onto the southern realm of the Turan continental domain.

In contrast, the chemistry of IAT sheeted dykes indicates that their tectonic setting of formation was characterized by no or negligible chemical influence from continental crust components, implying that these rocks formed onto the oceanic forearc sector of a continental arc. Alkaline rocks represent fragments of seamounts erupted in the subduction-unrelated oceanic basin and then tectonically accreted in the forearc setting.

ACKNOWLEDGEMENTS

The research was funded by the FAR-2017 and FAR-2018 Projects from the Ferrara University. R. Tassinari (University of Ferrara) is acknowledged for his technical support with chemical analyses. This paper has greatly benefited from constructive comments made by two anonymous reviewers.

REFERENCES

- Agard P., Omrani L., Jolivet L. and Mouthereau F., 2005. Convergence history across Zagros (Iran): constraints from collisional and earlier deformation. *Int. J. Earth Sci. (Geol. Rundsch)*, 94(380-398): 401-419, doi: 10.1007/s00531-005-0481-4.
- Aghanabati A., 2004. Major Sedimentary-Structural Units of Iran, Scale 2,500,000. *Geol. Surv. Min. Exp. Iran*.
- Alavi-Tehrani N., 1976. Geology and Petrography in the Ophiolitic Range NW of Sabzevar (Khorasan/Iran), with Special Regard to Metamorphism and Genetical Relations in an Ophiolite Suite. Thesis. University of Saarbrücken, 147 pp.
- Allahyari K., Saccani E., Pourmoafi M., Beccaluva L. and Masoudi F., 2010. Petrology of mantle peridotites and intrusive mafic rocks from the Kermanshah ophiolitic complex (Zagros belt, Iran): Implications for the geodynamic evolution of the Neo-Tethyan oceanic branch between Arabia and Iran. *Ophioliti*, 35: 71-90.
- Allahyari K., Saccani E., Rahimzadeh B. and Zeda O., 2014. Mineral chemistry and petrology of highly magnesian ultramafic cumulates from the Sarve-Abad (Sawlava) ophiolites (Kurdistan, NW Iran): New evidence for boninitic magmatism in intra-oceanic fore-arc setting in the Neo-Tethys between Arabia and Iran. *J. Asian Earth Sci.*, 79: 312-328, doi: 10.1016/j.jseas.2013.10.005.
- Allègre C.J. and Minster J.F., 1978. Quantitative models of trace element behavior in magmatic processes. *Earth Planet. Sci. Lett.*, 38: 1-25.
- Babaie H. A., Babaei A., Ghazi A. M. and Arvin M., 2006. Geochemical, $^{40}\text{Ar}/^{39}\text{Ar}$ age, and isotopic data for crustal rocks of the Neyriz ophiolite, Iran. *Canadian J. Earth Sci.*, 43: 57-70.
- Baroz F. and Macaudiere E.J., 1984. La serie volcanosedimentaire du chainon ophiolitique de Sabzevar (Iran). *Ophioliti*, 9: 3-26.
- Baroz F., Macaudiere J., Montigny R., Noghreyan M., Ohnenstetter M. and Rocci G., 1984. Ophiolites and related formations in the central part of the Sabzevar Range (Iran), and possible geotectonic reconstruction. *Neues Jahrbuch für Geologie und Paläontologie-Abhandlungen*, 168: 358-388.
- Barth M.G., Mason P.R.D., Davies G.R., Dijkstra A.H. and Drury M.R., 2003. Geochemistry of the Othris Ophiolite, Greece: evidence for refertilization?. *J. Petrol.*, 44: 1759-1785.
- Beccaluva L., Macciotta G., Piccardo G.B. and Zeda O., 1989. Clinopyroxene compositions of ophiolite basalts as petrogenetic indicator. *Chem. Geol.*, 77: 165-182.
- Beker J.A., Menzies M.A., Thirlwall M.F. and Macpherson C.G., 1997. Petrogenesis of Quaternary intraplate volcanism, Sana'a, Yemen: Implications for plume-Lithosphere interaction and polybaric melt hybridization. *J. Petrol.*, 38: 1359-1390.
- Bertrand P. and Mercier J.C.C., 1985-86. The mutual solubility of coexisting ortho- and clino-pyroxene: toward an absolute thermometer for the natural system?. *Earth Planet. Sci. Lett.*, 76: 109-122.
- Bortolotti V., Chiari M., Göncüoğlu M.C., Marcucci M., Principi G., Tekin U.K., Saccani E. and Tassinari R., 2013. Age and geochemistry of basalt-chert associations in the ophiolites of the Izmir-Ankara mélange east of Ankara, Turkey: preliminary data. *Ophioliti*, 38: 157-173, doi: 10.4454/phioliti.v38i2.424.
- Bortolotti V., Chiari M., Göncüoğlu M.C., Principi G., Saccani E., Tekin U.K. and Tassinari R., 2017. The Jurassic-Early Cretaceous Basalt-Chert association in the Ophiolites of the Ankara Mélange east of Ankara, Turkey: Age and Geochemistry. *Geol. Mag.*, p. 1-28, doi: <https://doi.org/10.1017/S0016756817000401>.
- Bortolotti V., Chiari M., Kodra A., Marcucci M., Mustafa F., Principi G. and Saccani E., 2004. New evidence for Triassic MORB magmatism in the northern Mirdita Zone ophiolites (Albania). *Ophioliti*, 29: 243-246.
- Bortolotti V., Marroni M., Nicolae I., Pandolfi L., Principi G. and Saccani E., 2002. Geodynamic implications of Jurassic ophiolites associated with island-arc volcanics, South Apuseni Mountains, western Romania. *Intern. Geol. Rev.*, 44: 938-955.
- Chauvet F., Lapierre H., Maury R.C., Bosch D., Basile C., Cotton J., Brunet P. and Campillo S., 2011. Triassic alkaline magmatism of the Hawasina Nappes: Post-breakup melting of the Oman lithospheric mantle modified by the Permian Neotethyan Plume. *Lithos*, 122: 122-136.
- Chiari M., Bortolotti V., Marcucci M., Photiades A., Principi G. and Saccani E., 2012. Radiolarian biostratigraphy and geochemistry of the Koziakas massif ophiolites (Greece). *Bull. Soc. Géol. France*, 183: 287-306.
- Delavari M., Dolati A., Marroni M., Pandolfi L. and Saccani E., 2016. Association of MORB and SSZ ophiolites along the shear zone between Coloured Mélange and Bajgan Complexes (North Maran, Iran): Evidence from the Sorkhband area. *Ophioliti*, 41: 21-34, doi: 10.4454/phioliti.v41i1.440.
- Dilek Y. and Furnes H., 2011. Ophiolite genesis and global tectonics: geochemical and tectonic fingerprinting of ancient oceanic lithosphere. *Geol. soc. Am. Bull.*, 123: 387-411. <http://dx.doi.org/10.1130/B30446.1>.
- Droop G.T.R., 1987. A general equation for estimating Fe^{3+} concentrations in ferromagnesian silicates and oxides from microprobe analyses, using stoichiometric criteria. *Mineral. Mag.*, 51: 431-435.
- Emami M.H., Sadeghi M.M. and Omrani S.J., 1993. Magmatic map of Iran, Scale 1:1,000,000. *Geol. Surv. Iran*.
- Ewart A., Bryan W.B., Chappell B.W. and Rudnick R.L., 1994. Regional Geochemistry of the Lau-Tonga Arc and Backarc Systems. In: J. Hawkins, L. Parson, J. Allan and et al. (Ed.), *Proceedings of the Ocean Drilling Program. Scientific Results 135, College Station, TX (Ocean Drilling Program)*, p. 385-425.
- Flower M.F.J. and Dilek Y., 2003. Arc-trench rollback and forearc accretion: 1. A collision-induced mantle flow model for Tethyan ophiolites. In: Y. Dilek and P.T. Robinson (Eds.), *Ophiolites in Earth History. Geol. Soc. London Spec. Publ.*, 218: 21-41.
- Gribble R.F., Stern R.J., Bloomer S.H., Stuben D., O'Hearn T. and Newman, S., 1996. MORB mantle and subduction components interact to generate basalts in the southern Mariana Trough back-arc basin. *Geochim. Cosmochim. Acta*, 60: 2153-2166.
- Hastie A.R., Kerr A.C., Pearce J.A. and Mitchell, S.F., 2007. Classification of altered volcanic island arc rocks using immobile trace elements: development of the Th Co discrimination diagram. *J. Petrol.*, 48: 2341-2357.
- Hébert R. and Laurent R., 1990. Mineral chemistry of the plutonic section of the Troodos ophiolite: new constraints for genesis of arc-related ophiolites. In: J. Malpas, E. Moores, A. Panayiotou and C. Xenophontos (Eds.), *Proceedings of the Troodos Ophiolite Symposium. Geol. Surv. Cyprus*, p. 149-163.
- Huene R. and Scholl D.W., 1991. Observations at convergent margins concerning sediment subduction, subduction erosion, and the growth of continental crust. *Rev. Geophys.*, 29: 279-316.
- Ionescu C., Hoeck V., Tomek C., Koller F., Balintoni I. and Lucian B., 2009. New insights into the basement of the Transylvanian Depression (Romania). *Lithos*, 108, 172-191, doi: 10.1016/j.lithos.2008.06.004.

- Irving A. J. and Frey F.A., 1984. Trace element abundances in megacrysts and their host basalts: constraints on partition coefficients and megacryst genesis. *Geochim. Cosmochim. Acta*, 48: 1201-1221.
- Khalatbari Jafari M., Babaie H.A. and Gani M., 2013a. Geochemical evidence for Late Cretaceous marginal arc-to-back arc transition in the Sabzevar ophiolitic extrusive sequence, northeast Iran. *J. Asian Earth Sci.*, 70-71: 209-230.
- Khalatbari Jafari M., Babaie H.A. and Mirzaie, M., 2013b. Geology, petrology and tectonomagmatic evolution of the plutonic crustal rocks of the Sabzevar ophiolite, NE Iran. *Geol. Mag.*, 150: 862-884.
- Koglin N., Kostopoulos D. and Reischmann T., 2009. Geochemistry, petrogenesis and tectonic setting of the Samothraki mafic suite, NE Greece: Trace-element, isotopic and zircon age constraints. *Tectonophysics*, 473: 53-68, doi: 10.1016/j.tecto.2008.10.028.
- Lachance G.R. and Trail, R.J., 1966. Practical solution to the matrix problem in X-ray analysis. *Canadian Spect.*, 11: 43-48.
- Lensch G. and Davoudzadeh M., 1982. Ophiolites in Iran. *Neues Jahrbuch für Geologie und Paläontologie-Monatshefte*, Stuttgart, 5: 306-320.
- Lensch G., Mihm A. and Alavi-Tehrani N., 1977. Petrography and geology of the ophiolite belt north of Sabzevar/Khorasan (Iran). *Neues Jahrbuch für Mineralogie, Abhandlungen*, 131: 156-178.
- Lensch G., Mihm A. and Alavi-Tehrani N., 1979. Major element geochemistry of the ophiolites north of Sabzevar (Iran). *Neues Jahrbuch für Geologie und Paläontologie Monatshefte*, 7: 415-447.
- Lensch G., Mihm A. and Alavi-Tehrani N., 1980. The post-ophiolitic volcanism north of Sabzevar/Iran: geology, petrography and major element geochemistry. *Neues Jahrbuch für Geologie und Paläontologie-Monatshefte*, Stuttgart, 11: 686-702.
- Letierrier J., Maury R.C., Thonon P., Girard D. and Marchal, M., 1982. Clinopyroxene composition as a method of identification of the magmatic affinities of paleo-volcanic series. *Earth Planet. Sci. Lett.*, 59: 139-154.
- Lindenberg H.G., Gorler K. and Ibbeken H., 1983. Stratigraphy, Structure and Orogenic Evolution of the Sabzevar Zone in the Area of Oryan (Khorasan, NE Iran). Report No., 51: 184-204.
- McCall G.J.H., 1997. The geotectonic history of the Makran and adjacent areas of southern Iran. *J. Asian Earth Sci.*, 15: 517-531.
- McKenzie D. and O'Nions, R.K., 1991. Partial melt distributions from inversion of rare earth element concentrations. *J. Petrol.*, 32: 1021-1091.
- Morimoto N. 1989. Nomenclature of pyroxenes. *Canadian Mineral.*, 27: 143-156.
- Moslempour M. E., Khalatbari-Jafari M. and Ghaderi M., 2015. Petrology, Geochemistry and Tectonics of the Extrusive Sequence of Fannuj-Maskutan Ophiolite, Southeastern Iran. *J. Geol. Soc. India*, 85: 604-618.
- Murton B.J., 1989. Tectonic controls on boninite genesis. In: A.D. Saunders and M.J. Norry, (Ed.), *Magmatism in the Ocean Basins*: Geol. Soc. London Spec. Publ., 42: 347-377.
- Najafzadeh A. R., Arvin M., Pan Y. and Ahmadipour H., 2008. Podiform Chromitites in the Sorkhband Ultramafic Complex, Southern Iran: Evidence for Ophiolitic Chromitite. *J. Sci., Islamic Republic Iran*, 19: 49-65.
- Nicolae I. and Saccani E., 2003. Petrology and geochemistry of the Late Jurassic calc-alkaline series associated to Middle Jurassic ophiolites in the South Apuseni Mountains (Romania). *Swiss Jour. Petrol.*, 83: 81-96.
- Noghreyan M., 1982. Evolution géochimique, mineralogique et structurale d'un édifice ophiolitique singulier: le massif de Sabzevar (partie centrale), NE de l'Iran, These Doc. d'Etat, Université de Nancy I, France, 239 pp.
- Ohnenstetter M., 1980. Sur la signification des sutures ophiolitiques en fonction de leurs caractères structuraux. *C. R. Acad. Sci., Paris*, 291, série D: 741-743.
- Ohnenstetter M., 1983. The role of possible transverse faults in the development of the Sabzevar ophiolites, northeast Iran, with special reference to magma chamber tectonics. *Sci. Geol. Bull.*, 36: 73-90.
- Omrani H., Moazzen M., Oberhansli R., Altenberger U. and Lange M., 2013. The Sabzevar blueschists of the North-Central Iranian micro-continent as remnants of the Neotethys related oceanic crust subduction. *Inter. J. Earth Sci.*, 102: 1491-1512, <http://dx.doi.org/10.1007/s00531-013-0881-9>.
- Omrani H., Moazzen M., Oberhansli R. and Molslempour M.E., 2017. Iranshahr blueschist: subduction of the inner Makran oceanic crust. *J. Metamorphic Geol.*, 35: 373-392. doi: 10.1111/jmg.12236.
- Parkinson I.J. and Pearce J.A., 1998. Peridotites from the Izu-Bonin-Mariana forearc (ODP Leg 125): evidence for mantle melting and melt-mantle interaction in a suprasubduction zone setting. *J. Petrol.*, 39: 1577-1618.
- Parlak O., Rizaoglu T., Bağcı U., Karaoglan F. and Hoeck, V., 2009. Tectonic significance of the geochemistry and petrology of ophiolites in southeast Anatolia, Turkey. *Tectonophysics*, 473: 173-187, <http://dx.doi.org/10.1016/j.tecto.2008.08.002>.
- Pearce J.A., 1982. Trace element characteristics of lavas from destructive plate boundaries. In: R.S. Thorpe (Ed.), *Andesites*. Wiley, New York, p. 525-548.
- Pearce J.A., 1983. Role of the Sub-continental Lithosphere in Magma Genesis at Active Continental Margin. In: C.J. Hawkesworth and M.J. Norry (Ed.), *Continental basalts and mantle xenoliths*. Nantwich, Cheshire, Shiva Publ., p. 230-249.
- Pearce J.A., 1996. A user's guide to basalt discrimination diagrams. In: A.H. Bailes, E.H. Christiansen, A.G. Galley, G.A. Jenner, J.D. Keith, R. Kerrich, D.R. Lentz, C.M. Lesher, S.B. Lucas, J.N. Ludden, J.A. Pearce, S.A. Peloquin, R.A. Stern, W.E. Stone, E.C. Syme, H.S. Swinden and D.A. Wyman (Ed.), *Trace element geochemistry of volcanic rocks: applications for massive sulphide exploration*. Short Course Notes. Geol. Assoc. Canada, 12: 79-113.
- Pearce J.A. and Norry M.J., 1979. Petrogenetic implications of Ti, Zr, Y, and Nb variations in volcanic rocks. *Contrib. Mineral. Petrol.*, 69: 33-47.
- Pearce J.A. and Parkinson I.J., 1993. Trace element models for mantle melting: Application to volcanic arc petrogenesis. *Geol. Soc. London Spec. Publ.*, 76: 373-403, doi: 10.1144/GSL.SP.1993.076.01.19.
- Putirka K.D., 2008. Thermometers and barometers for volcanic systems. In: K.D. Putirka and F. Tepley (Ed.), *Mineral inclusions and volcanic processes*. Review in *Mineralogy and Geochemistry*. Am. Mineral. Soc., Washington DC., 69: 61-120.
- Rolland Y., Galoyan G., Bosch D., Sosson M., Corsini M., Fornari M. and Vèrati C., 2009. Jurassic Back-arc and hot-spot related series in the Armenian ophiolites -Implications for the obduction process. *Lithos*, 112: 163-187, doi: 10.1016/j.lithos.2009.02.006.
- Rossetti F., Nasrabad M., Vignaroli G., Theye T., Gerdes A., Razavi M. and Moin Vaziri H., 2009. Early Cretaceous migmatitic mafic granulites from the Sabzevar range (NE Iran): Implications for the closure of the Mesozoic peri-Tethyan oceans in central Iran. *Terra Nova*, 22: 26-34.
- Saccani E., 2015. A new method of discriminating different types of post-Archean ophiolitic basalts and their tectonic significance using Th-Nb and Ce-Dy-Yb systematics. *Geosci. Frontiers*, 6: 481-501.
- Saccani E., Allahyari K., Beccaluva L. and Bianchini G., 2013. Geochemistry and petrology of the Kermanshah ophiolites (Iran): Implication for the interaction between passive rifting, oceanic accretion, and plume-components in the Southern Neotethys Ocean. *Gondwana Res.*, 24: 392-411, <http://dx.doi.org/10.1016/j.gr.2012.10.009>.
- Saccani E., Allahyari K. and Rahimzadeh B., 2014. Petrology and geochemistry of mafic magmatic rocks from the Sarve-Abad ophiolites (Kurdistan region, Iran): Evidence for interaction between MORB-type asthenosphere and OIB-type components in the southern Neo-Tethys Ocean. *Tectonophysics*, 621: 132-147, doi:10.1016/j.tecto.2014.02.011.

- Saccani E., Beccaluva L., Photiades A. and Zeda O., 2011. Petrogenesis and tectono-magmatic significance of basalts and mantle peridotites from the Albanian-Greek ophiolites and sub-ophiolitic mélanges. New constraints for the Triassic-Jurassic evolution of the Neo-Tethys in the Dinaride sector. *Lithos*, 124: 227-242, doi:10.1016/j.lithos.2010.10.009.
- Saccani E., Bortolotti V., Marroni M., Pandolfi L., Photiades A. and Principi G., 2008a. The Jurassic association of backarc basin ophiolites and calc-alkaline volcanics in the Guevgueli Complex (northern Greece): Implication for the evolution of the Vardar Zone. *Ophioliti*, 33: 209-227.
- Saccani E., Delavari M., Beccaluva L. and Amini S.A., 2010. Petrological and geochemical constraints on the origin of the Nehbandan ophiolitic complex (eastern Iran): Implication for the evolution of the Sistan Ocean. *Lithos*, 117: 209-228.
- Saccani E., Delavari M., Dolati A., Marroni M., Pandolfi L., Chiari M. and Barbero E., 2017. New insights into the geodynamics of Neo-Tethys in the Makran area: Evidence from age and petrology of ophiolites from the Coloured Mélange Complex (SE Iran). *Gondwana Res.*: <http://dx.doi.org/10.1016/j.gr.2017.07.013>.
- Saccani E., Dilek Y., Marroni M. and Pandolfi L., 2015. Continental margin ophiolites of Neotethys: Remnants of Ancient Ocean-Continent Transition Zone (OCTZ) lithosphere and their geochemistry, mantle sources and melt evolution patterns. *Episodes*, 38: 230-249.
- Saccani E., Photiades A. and Beccaluva L., 2008b. Petrogenesis and tectonic significance of IAT magma-types in the Hellenide ophiolites as deduced from the Rhodiani ophiolites (Pelagonian zone, Greece). *Lithos*, 104: 71-84.
- Saccani E., Photiades A. and Padoa E., 2003. Geochemistry, petrogenesis and tectono-magmatic significance of volcanic and sub-volcanic rocks from the Koziakas Mélange (Western Thessaly, Greece). *Ophioliti*, 28: 43-57.
- Sahandi R., 1993. Geological Map of Sabzevar Quadrangle, Scale 1:250,000. *Geol. Surv. Min. Exp. Iran*.
- Salavati M., 2008. Petrology, geochemistry and mineral chemistry of extrusive alkalic rocks of the Southern Caspian sea ophiolite, Northern Alborz, Iran: evidence of alkaline magmatism in Southern Eurasia. *Jour. Applied Sci.*, 8: 2202-2216.
- Schilling J.G., Zajac M., Evans R., Johnston T., White W., Devine J.D. and Kingsley R., 1983. Petrologic and geochemical variations along the Mid-Atlantic Ridge from 29°N to 73°N. *Am. J. Sci.*, 283: 510-586.
- Sengor A.M.C., 1990. A new model for the late Paleozoic-Mesozoic tectonic evolution of Iran and implication for Oman. In: A.H.F. Robertson, M.P. Searle and A.C. Rise (Ed.), *The Geology and Tectonics of the Oman Region*. *Geol. Soc. London, Spec. Publ.*, 49: 797-831.
- Shafaii-Moghadam H., Corfu F., Chiaradia M., Stern R. J., Ghorbani Gh., 2014. Sabzevar Ophiolite, NE Iran: Progress from embryonic oceanic lithosphere into magmatic arc constrained by new isotopic and geochemical data. *Lithos*, 210-211: 224-241.
- Shafaii-Moghadam H., Mosaddegh H. and Santosh M., 2013. Geochemistry and petrogenesis of the Late Cretaceous Haji-Abad ophiolite (Outer Zagros Ophiolite Belt, Iran): Implications for geodynamics of the Bitlis-Zagros suture zone. *Geol. J.*, 48: 579-602.
- Shafaii-Moghadam H., Whitechurch H., Rahgoshay M. and Monsef I., 2009. Significance of Nain-Baft ophiolitic belt (Iran): Short-lived, transtensional Cretaceous back-arc oceanic basins over the Tethyan subduction zone. *C. R. Geosci.*, 341: 1016-1028.
- Sheikholeslami M. R., Pique A., Mobayen P., Sabzehei M., Bellon H. and Emami M. H., 2008. Tectono-metamorphic evolution of the Neyriz metamorphic complex, Quri-Kor-e-Sefid area (Sanandaj-Sirjan Zone, SW Iran). *J. Asian Earth Sci.*, 31: 504-521.
- Shojaat B., Hassanipak A.A., Mobasher K., Ghazi A.M., 2003. Petrology, geochemistry and tectonics of the Sabzevar ophiolite, North Central Iran. *J. Asian Earth Sci.*, 21: 1053-1067.
- Spies O., Lensch G. and Mihem A., 1983. Geochemistry of the post-ophiolitic Tertiary volcanics between Sabzevar and Quchan (NE Iran). *Geol. Surv. Iran, Report No. 51*: 247-266.
- Stöcklin J., 1974. Possible ancient continental margins in Iran. In: C.A. Burk and C.L. Drake, (Ed.), *The geology of continental margins*. Springer-Verlag, New York, p. 873-887.
- Sun S.S. and McDonough W.F., 1989. Chemical and isotopic systematics of oceanic basalts: Implications for mantle composition and processes. In: A.D. Saunders and M.J. Norry, (Ed.), *Magmatism in Ocean Basins*. *Geol. Soc. London Spec. Publ.*, 42: 313-345.
- Takin M., 1972. Iranian geology and continental drift in the Middle East. *Nature*, 235: 147-150.
- Taylor S.R. and McLennan S.M., 1985. *The Continental Crust: its composition and evolution: an examination of the geochemical record preserved in sedimentary rocks*. Oxford, Blackwell Scientific Publication, 312 pp.
- Thirlwall M., Upton B.G.J. and Jenkins C., 1994. Interaction between continental lithosphere and the Iceland plume: Sr-Nd-Pb isotope geochemistry of Tertiary basalts, NE Greenland. *J. Petrol.*, 35: 839-879.
- Tirrul R., Bell I. R., Griffis R. J. and Camp V. E., 1983. The Sistan suture zone of eastern Iran. *Geol. Soc. Am. Bull.*, 94: 134-150.
- Valsami E. and Cann J.R., 1992. Mobility of rare earth elements in zones of intense hydrothermal alteration in the Pindos ophiolite, Greece. In: L.M. Parson, B.J. Murton and P. Browning (Ed.), *Ophiolites and their modern oceanic analogues*. *Geol. Soc. London Spec. Publ.*, 60: 219-232.
- Winchester J.A. and Floyd P.A., 1977. Geochemical discrimination of different magma series and their differentiation products using immobile elements. *Chem. Geol.* 20: 325-343.
- Yuan C., Sun M., Zhou M.F., Xiao W. and Zhou H., 2005. Geochemistry and petrogenesis of the Yishak Volcanic Sequence, Kudi ophiolite, West Kunlun (NW China): Implications for the magmatic evolution in a subduction zone environment. *Contrib. Mineral. Petrol.*, 150: 195-211, doi: 10.1007/s00410-005-0012-0.

Received, January 2, 2018

Accepted, May 4, 2018

Appendix A. Comparison of major (wt.%) and trace element (ppm) concentrations in reference samples analyzed using X-Ray Fluorescence spectrometry (XRF) and Inductively Coupled Plasma-Mass Spectrometry (ICP-MS).

	BE-N			BHVO-1			Detection limit
	Recomm.	Measured	Relative error (%)	Recomm.	Measured	Relative error (%)	
<i>XRF:</i>							
SiO ₂	38.48	38.72	-0.6	49.94	49.62	0.6	0.05
TiO ₂	2.63	2.59	1.5	2.71	2.74	-1.1	0.01
Al ₂ O ₃	10.14	9.82	3.2	13.80	13.95	-1.1	0.05
Fe ₂ O ₃	12.93	12.66	2.1	12.23	12.60	-3.0	0.10
MnO	0.20	0.19	7.4	0.17	0.16	5.9	0.05
MgO	13.25	13.42	-1.3	7.23	7.44	-2.9	0.01
CaO	13.97	14.11	-1.0	11.40	11.36	0.4	0.04
Na ₂ O	3.20	3.31	-3.3	2.26	2.36	-4.4	0.01
K ₂ O	1.40	1.36	2.9	0.52	0.49	5.8	0.01
P ₂ O ₅	1.06	1.01	4.5	0.27	0.25	7.4	0.01
Zn	120	122	-1.7	105	100	4.8	3
Cu	72	73	-0.8	136	141	-3.7	3
Sc	22	20	9.1	31.8	30	5.7	3
Ga	17	16	4.4	21	22	-4.8	4
Ni	267	259	3.0	121	118	2.5	2
Co	60	62	-3.3	45	46	-2.2	2
Cr	360	354	1.7	289	281	2.8	2
V	235	238	-1.3	317	322	-1.6	2
Ba	1025	997	2.7	139	144	-3.6	3
Rb	47	46	2.1	11	10	9.1	1
Sr	1370	1358	0.9	403	410	-1.7	2
Y	30	29	3.3	27.6	27	2.2	2
Zr	260	266	-2.3	179	174	2.8	2
La	82	79	3.7	15.8	18	-13.9	5
Ce	152	159	-4.6	39	41	-5.1	5
Nd	67	65	3.7	25.2	26	-3.2	4
Nb	105	102	2.9	19	20	-5.3	1
Th	10.4	11	-2.7	1.08	1	7.4	1
Pb	4	5	-25.0	2.6	n.d.		4
<i>ICP-MS:</i>							
Rb				11	11.2	-1.8	0.02
Sr				403	392	2.7	0.02
Y				27.6	27.1	1.8	0.003
Zr				179	187	-4.5	0.02
La				15.8	16.0	-1.2	0.051
Ce				39	37.9	2.8	0.051
Pr				5.7	5.84	-2.5	0.009
Nd				25.2	25.9	-2.8	0.023
Sm				6.2	6.44	-3.9	0.004
Eu				2.06	2.01	2.4	0.05
Gd				6.4	6.31	1.4	0.007
Tb				0.96	0.943	1.8	0.057
Dy				5.2	5.35	-2.9	0.002
Ho				0.99	1.02	-3.0	0.046
Er				2.4	2.49	-3.8	0.005
Tm				0.33	0.341	-3.3	0.017
Yb				2.02	2.08	-3.0	0.01
Lu				0.291	0.308	-5.8	0.012
Nb				19	18.5	2.6	0.01
Hf				4.38	4.32	1.4	0.007
Ta				1.23	1.30	-5.7	0.026
Th				1.08	1.11	-2.8	0.007
U				0.42	0.41	2.86	0.03

Recommended (Recomm.) values for international reference materials BE-N and BHVO-1 are from K. Govindaraju (1994) Geostandard Newsletter, Special Issue, v. 118, 158 p. Detection limits for XRF and ICP-MS analyses were determined using 29